nature communications

Article

https://doi.org/10.1038/s41467-024-54819-5

ABHD6 loss-of-function in mesoaccumbens postsynaptic but not presynaptic neurons prevents diet-induced obesity in male mice

Received: 22 January 2024

Accepted: 22 November 2024

Published online: 16 December 2024

Check for updates

David Lau[1,2,6], Stephanie Tobin[1,6], Horia Pribiag[3], Shingo Nakajima[1], Alexandre Fisette[1], Dominique Matthys[1,2], Anna Kristyna Franco Flores[1,2], Marie-Line Peyot[1], S. R. Murthy Madiraju[1], Marc Prentki[1,4], David Stellwagen[3], Thierry Alquier[1,5] & Stephanie Fulton[1,4]

α/β-hydrolase domain 6 (ABHD6) is a lipase linked to physiological functions affecting energy metabolism. Brain ABHD6 degrades 2-arachidonoylglycerol and thereby modifies cannabinoid receptor signalling. However, its functional role within mesoaccumbens circuitry critical for motivated behaviour and considerably modulated by endocannabinoids was unknown. Using three viral approaches, we show that control of the nucleus accumbens by neuronal ABHD6 is a key determinant of body weight and reward-directed behaviour in male mice. Contrary to expected outcomes associated with increasing endocannabinoid tone, loss of ABHD6 in nucleus accumbens, but not ventral tegmental area, neurons completely prevents diet-induced obesity, reduces food- and drug-seeking and enhances physical activity without affecting anxiodepressive behaviour. These effects are explained by attenuated inhibitory synaptic transmission onto medium spiny neurons. ABHD6 deletion in nucleus accumbens neurons and dopamine ventral tegmental area neurons produces contrasting effects on effortful responding for food. Intraventricular infusions of an ABHD6 inhibitor also restrain appetite and promote weight loss. Together, these results reveal functional specificity of pre- and post-synaptic mesoaccumbens neuronal ABHD6 to differentially control energy balance and propose ABHD6 inhibition as a potential anti-obesity tool.

Endocannabinoids regulate numerous facets of physiology and behaviour[1], and human studies have consistently reported that *CNR1* (CB1R) is among the genetic candidates with strong association to obesity[2]. In the sixteen years since the withdrawal of the anti-obesity drug Rimonabant (CB1R inverse agonist) due to serious mood deficits, research has advanced in the search for more refined cellular- and subcellular-specific mechanisms controlling endocannabinoid signalling. α/β hydrolase domain 6 (ABHD6) is a monoacylglycerol hydrolase with diverse physiological roles[3]. Within the brain, postsynaptically localized neuronal ABHD6 contributes to the degradation of the endocannabinoid 2-arachidinoylglycerol (2-AG) at its site of synthesis. Thus, ABHD6 regulates the accumulation of 2-AG and consequent signalling at presynaptic type 1 cannabinoid receptors (CB1R)[4,5], positioning ABHD6 as a component of the endocannabinoid system (ECS)[6].

The mesoaccumbens pathway comprises midbrain dopamine (DA) neurons originating in the ventral tegmental area (VTA) with

[1]Centre de Recherche du Centre Hospitalier de l'Université de Montréal (CRCHUM), Montréal, QC, Canada. [2]Department of Neuroscience, Université de Montréal, Montréal, QC, Canada. [3]Department of Neurology and Neurosurgery, Centre for Research in Neuroscience, McGill University Health Center, Montréal, QC, Canada. [4]Department of Nutrition, Université de Montréal, Montréal, QC, Canada. [5]Department of Medicine, Université de Montréal, Montréal, QC, Canada. [6]These authors contributed equally: David Lau, Stephanie Tobin. e-mail: stephanie.fulton@umontreal.ca

projections to postsynaptic targets in the nucleus accumbens (NAc), and represents a critical neural substrate regulating effortful and motoric behaviour and encoding action outcomes[7,8]. Endocannabinoid regulation of motivation is well linked to 2-AG/CB1R signalling in mesoaccumbens circuitry[9–12]. 2-AG release from VTA DA neurons targets presynaptic CB1Rs localized on VTA GABAergic and glutamatergic terminals[13–15], with CB1R signalling on GABAergic terminals promoting DA neuron disinhibition and increased DA release in the NAc[16–19]. VTA 2-AG/CB1R signalling thus controls accumbal DA dynamics[20–24] to sustain behaviours oriented towards acquisition of palatable food and cue-induced invigoration of behaviour[25–29].

Within the NAc, DA release modulates the activity of dopaminoceptive GABAergic medium spiny neurons (MSNs), which comprise the vast majority of neurons in this structure[30]. However, MSN activity is additionally modulated by endocannabinoid signalling within the NAc[31–33], whereby 2-AG released from MSNs targets CB1Rs expressed on presynaptic corticolimbic glutamatergic inputs[34–37] and local GABAergic fast-spiking interneurons[38–43]. Suggesting potential for ABHD6 to participate in mesoaccumbens circuit function, pharmacological inhibition of ABHD6 has been demonstrated to enhance striatal 2-AG content and regulate nicotine-induced changes in GABAergic input to VTA DA neurons[44]. However, the precise functional role of ABHD6 within the mesoaccumbens circuitry remained unknown. Considering the robust expression of CB1R within basal ganglia circuits[45], its important role in food-directed behaviour[8], and potential for such processes to be disrupted by interactions between genetics and obesogenic environments[46], deciphering the impact of ABHD6 function within the VTA and NAc provides new insights into the intricate manner through which the ECS regulates feeding, body weight, and motivated behaviour.

In contrast to the canonical, presynaptically-localized 2-AG degrading enzyme MAGL, ABHD6 is localized postsynaptically at the site of 2-AG synthesis[5] and is uniquely positioned to control 2-AG spatiotemporal accumulation. To investigate the role of mesoaccumbal ABHD6, we harnessed three cell-specific viral gene knockout approaches in adult mice to determine ABHD6 function in NAc and VTA neurons. This approach provided a cell-type and site-specific vantage to examine endogenous endocannabinoid signalling within a physiological range while avoiding potential confounding effects associated with manipulation of 2-AG/cannabinoid receptor signalling during development[47,48].

Opposing the well-described impact of increased endocannabinoid tone to promote energy accumulation, hypolocomotion, and stimulate goal-oriented behaviour[9,10,49,50], we demonstrate that NAc neuronal ABHD6 deletion blunts reward-directed behaviour and is highly protective against diet-induced obesity and associated sedentary behaviour. By comparison, VTA neuronal ABHD6 deletion reduced spontaneous locomotor activity on HFD, while VTA DA-neuron specific ABHD6 invalidation heightened food-motivated behaviour in an energy-state dependent manner.

Results

Nucleus accumbens neuronal ABHD6 loss-of-function reduces body weight and stimulates locomotor activity on a chow diet

Abhd6 mRNA was robustly expressed within NAc cells, including *Slc32a1*-expressing GABAergic neurons (Fig. 1a), consistent with recent RNA-seq findings[51,52]. To explore the role of NAc neuronal ABHD6 function, a Cre-Lox, viral-mediated approach was used to conditionally knockout ABHD6 from NAc neurons[53]. Synapsin-promotor adeno-associated viruses expressing GFP (AAV-hSyn-GFP) or Cre recombinase (AAV-hSyn-Cre) were bilaterally injected into the NAc of adult male *Abhd6*$^{lox/lox}$ mice[54], to generate ABHD6$^{NAc\ GFP}$ and ABHD6$^{NAc\ KO}$ mice (Fig. 1b). Viral expression with specificity for NAc neurons and conditional deletion of ABHD6 was verified by immunostaining and reduced NAc *Abhd6* expression (Fig. 1c, d). Conditional NAc neuronal ABHD6 loss-of-function was associated with reduced expression of *Cnr1*, without impacting the expression of the 2-AG hydrolyzing enzyme monoacylglycerol lipase (*Mgll*) (Fig. 1d). No differences were observed in diacylglycerol lipase-alpha (*Dagla*) or -beta (*Daglb*) expression (Supplementary Fig. 1a), suggesting *Abhd6* invalidation did not result in compensatory changes in the expression of 2-AG biosynthetic enzymes. NAc expression of both *Faah* and *Napepld* was reduced in ABHD6$^{NAc\ KO}$ mice (Supplementary Fig. 1a). Our neuron-specific conditional deletion approach did not result in complete loss of NAc *Abhd6* expression, in agreement with expression of *Abhd6* in glia of the striatum[51,55]. Consistent with activity of ABHD6 to preferentially degrade 2-AG, levels of NAc 2-AG, but not anandamide, were significantly augmented in ABHD6$^{NAc\ KO}$ mice (Fig. 1e). The magnitude of this increase in 2-AG (~1.8 fold increase) is within physiological range and is modest compared to the over 10-fold increases in 2-AG observed following monoacylglycerol lipase (MAGL) inhibition[56].

First, we sought to determine the impact of neuronal ABHD6 loss-of-function in the NAc on energy metabolism by measuring body weight and food intake, and other metabolic endpoints in adult mice consuming a standard chow diet for 8 weeks. ABHD6$^{NAc\ KO}$ mice exhibited reduced body weight gain (Fig. 1f), lean mass, and fat mass (Fig. 1g), with no differences in body length (Supplementary Fig. 1b). Free-feeding chow intake was not different between ABHD6$^{NAc\ GFP}$ and ABHD6$^{NAc\ KO}$ mice (Fig. 1h), with feed efficiency reduced in ABHD6$^{NAc\ KO}$ mice (Fig. 1i). No differences in energy expenditure were observed (Supplementary Fig. 1c, d), and a trend towards an elevated respiratory exchange ratio (RER) in ABHD6$^{NAc\ KO}$ mice was observed during the dark cycle (Supplementary Fig. 1e, f). Spontaneous locomotor activity was increased in ABHD6$^{NAc\ KO}$ mice with significant increases apparent in the light cycle (Fig. 1j, k). Given evidence implicating engagement of the endocannabinoid system by exercise[57], and the functional role of endocannabinoid system in the rewarding effects of running[58–60], we next assessed whether NAc neuronal ABHD6 loss-of-function may enhance voluntary wheel-running. Wheel-running behaviour and body weight were unchanged on the standard chow diet (Fig. 1l, m; Supplementary Fig. 1g).

ABHD6 deletion in nucleus accumbens neurons attenuates motivation for sugar and context-conditioned reward without affecting anxiodepressive behaviour

Endocannabinoid signalling within the NAc is known to regulate motivated behaviour[11,12,61], thus we hypothesized that ABHD6 would affect effortful responding for sucrose and context-conditioned approach. To explore food-motivated behaviour, mice were trained on an operant task for sugar rewards (Fig. 2a, Supplementary Fig. 2a, b). ABHD6$^{NAc\ KO}$ mice displayed decreased responding indicating blunted food-motivated behaviour (Fig. 2b, c). We additionally tested mice in an amphetamine conditioned place preference test as a readout of mesoaccumbens function (Fig. 2d). ABHD6$^{NAc\ KO}$ mice exhibited decreased conditioned approach behaviour to a context paired with drug reward (Fig. 2e). In view of these results and evidence linking the ECS to mood regulation[34,62–65], we also assessed anxiety-like behaviour in the open field test and elevated plus maze, and despair-like behaviour using the forced swim task. No changes were observed (Fig. 2f–l) suggesting dampened reward-driven behaviours are not due to altered mood states.

Nucleus accumbens neuronal ABHD6 loss-of-function prevents diet-induced obesity and physical inactivity

Next, we studied changes in energy metabolism induced by a saturated HFD. Weight gain was strongly reduced in ABHD6$^{NAc\ KO}$ mice relative to controls (Fig. 3a), accompanied by a corresponding reduction in fat mass (Fig. 3b). A trend towards reduced cumulative food intake on HFD was observed in ABHD6$^{NAc\ KO}$ mice (Fig. 3c, Supplementary

https://doi.org/10.1038/s41467-024-54819-5

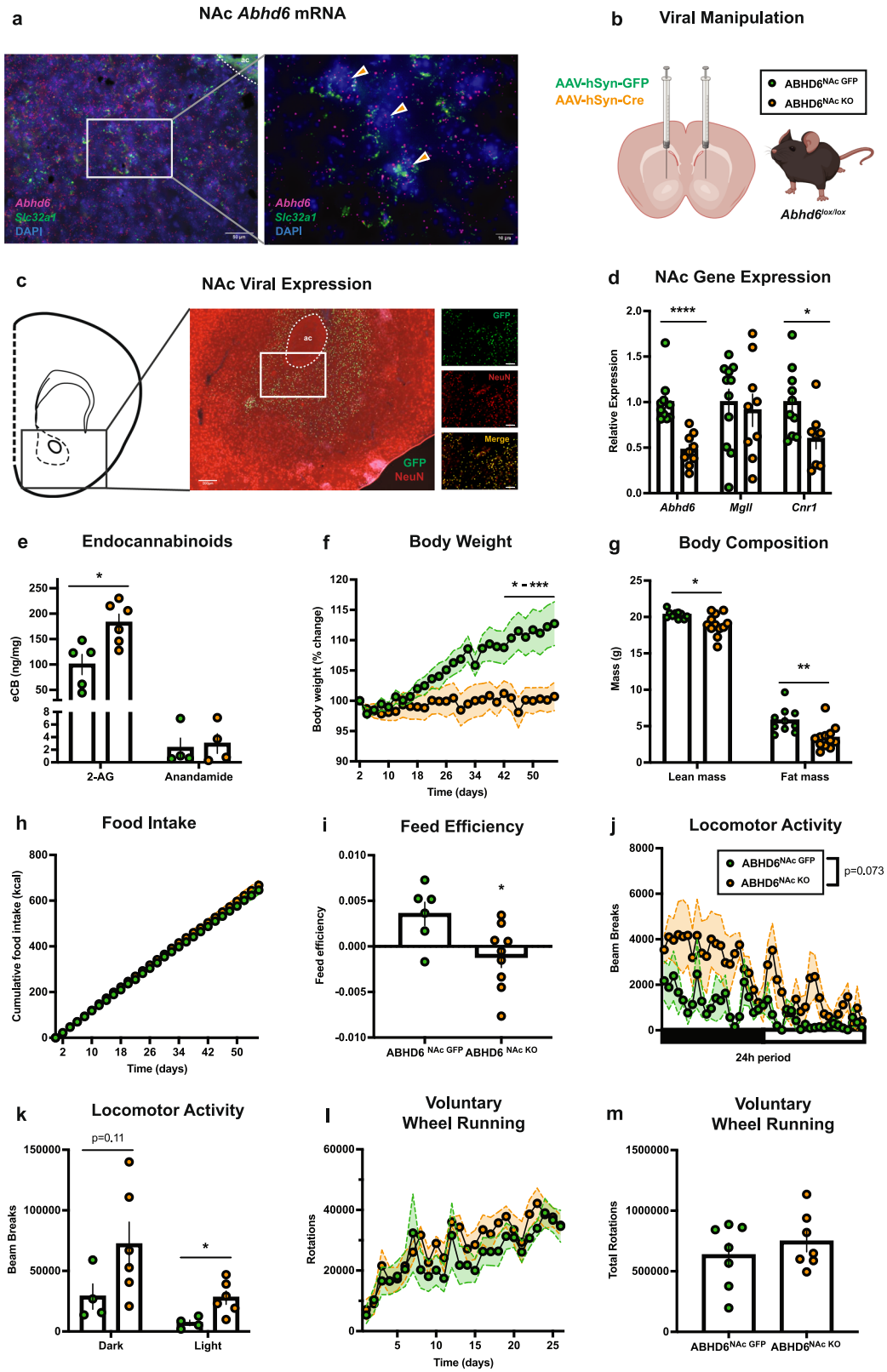

Fig. 3a), with reduced feed efficiency (Fig. 3d). No differences in RER or energy expenditure were observed (Fig. 3e–h). Overall spontaneous locomotor activity was increased in ABHD6$^{NAc\ KO}$ mice (Fig. 3i, j). Diet-induced obesity leads to decreases in voluntary exercise[66]. Thus, considering increases in locomotion in ABHD6$^{NAc\ KO}$ mice, we evaluated voluntary wheel-running in a separate cohort of animals following 8 weeks of HFD. While ABHD6$^{NAc\ GFP}$ controls showed markedly reduced wheel running activity in response to diet-induced obesity, ABHD6$^{NAc\ KO}$ mice exhibited robust wheel-running (Fig. 3k–l) at levels approximating chow-fed controls (Supplementary Fig. 3b, c), suggesting that NAc neuronal ABHD6 loss-of-function prevents inactivity resulting from diet-induced obesity.

Fig. 1 | ABHD6 loss-of-function in nucleus accumbens neurons suppresses body weight gain and increases locomotor activity. a Photomicrograph of NAc showing representative in situ hybridization labelling of *Slc32a1* (GABA transporter, green) and *Abhd6* (red) probes of 6 experiments from 2 mice. Orange arrows indicate cells with co-localization of *Slc32a1* and *Abhd6* expression. ac, anterior commissure. **b** Schematic of viral manipulation. Created in BioRender. Lau, D. (2023) BioRender.com/w94o015. **c** Representative photomicrograph of NAc viral expression from AAV-hSyn-GFP-injected mouse (centre). Representative photomicrograph of NAc viral expression illustrating colocalization of GFP and NeuN (right), of 4 experiments from 2 mice. Scale bar 200 µm (left), 50 µm (right). **d** NAc gene expression of *Abhd6* ($ABHD6^{NAc\ GFP}$: n = 10, $ABHD6^{NAc\ KO}$: n = 9, P < 0.0001), *Mgll* ($ABHD6^{NAc\ GFP}$: n = 11, $ABHD6^{NAc\ KO}$: n = 9, P = 0.6964), and *Cnr1* ($ABHD6^{NAc\ GFP}$: n = 10, $ABHD6^{NAc\ KO}$: n = 8, P = 0.0277). **e** NAc 2-AG ($ABHD6^{NAc\ GFP}$: n = 5, $ABHD6^{NAc\ KO}$: n = 6, P = 0.0111) and anandamide levels ($ABHD6^{NAc\ GFP}$: n = 4, $ABHD6^{NAc\ KO}$: n = 4, P = 0.7732). **f** Body weight ($ABHD6^{NAc\ GFP}$: n = 8, $ABHD6^{NAc\ KO}$: n = 7, two-way ANOVA interaction P < 0.0001). **g** Lean ($ABHD6^{NAc\ GFP}$: n = 10, $ABHD6^{NAc\ KO}$: n = 12, P = 0.0120) and fat mass ($ABHD6^{NAc\ GFP}$: n = 10, $ABHD6^{NAc\ KO}$: n = 12, P = 0.0031). **h** Food intake ($ABHD6^{NAc\ GFP}$: n = 6, $ABHD6^{NAc\ KO}$: n = 9, two-way ANOVA interaction P = 0.9889). **i** Feed efficiency ($ABHD6^{NAc\ GFP}$: n = 6, $ABHD6^{NAc\ KO}$: n = 9, P = 0.0208). **j** Locomotor activity ($ABHD6^{NAc\ GFP}$: n = 4, $ABHD6^{NAc\ KO}$: n = 6, two-way ANOVA group main effect P = 0.0729). **k** Locomotor activity in (**j**) during dark ($ABHD6^{NAc\ GFP}$: n = 4, $ABHD6^{NAc\ KO}$: n = 6, P = 0.01148) and light cycle ($ABHD6^{NAc\ GFP}$: n = 4, $ABHD6^{NAc\ KO}$: n = 6, P = 0.0196). **l** Wheel-running ($ABHD6^{NAc\ GFP}$: n = 7, $ABHD6^{NAc\ KO}$: n = 7, two-way ANOVA interaction P = 0.6674). **m** Cumulative wheel-running from (**l**) ($ABHD6^{NAc\ GFP}$: n = 7, $ABHD6^{NAc\ KO}$: n = 7, P = 0.4085). Data represented as mean ± SEM; *p < 0.05, **p < 0.01, ***p < 0.001, ****p < 0.0001. Unpaired two-sided t-test (**d**, **e**, **g**, **i**, **k**, **m**), two-way ANOVA group x time interaction with Sidak's post hoc correction (**f**), two-way ANOVA group x time interaction (**h, l**), two-way ANOVA group main effect (**j**). Additional details on statistical tests are available in the Supplementary Information. Source data are provided as a Source Data file. Created in BioRender. Lau, D. (2023) BioRender.com/w94o015.

Nucleus accumbens neuronal ABHD6 loss-of-function reduces synaptic inhibitory transmission onto medium spiny neurons

To investigate the impact of NAc neuronal ABHD6 deletion on NAc synaptic physiology, patch-clamp recordings from medium spiny neurons (MSNs) of the NAc were collected from slices (Fig. 4a). Miniature inhibitory postsynaptic current (mIPSC) frequency and amplitude were both reduced in MSNs from $ABHD6^{NAc\ KO}$ mice (Fig. 4b, c). Consistent with this, both spontaneous IPSC frequency and amplitude were significantly lower in MSNs from $ABHD6^{NAc\ KO}$ mice (Fig. 4d, e). In contrast to sIPSC results, no differences in sEPSC frequency or amplitude were observed (Fig. 4f, g).

To examine the impact of exogenous CB1R stimulation, a CB1R agonist (WIN55,212-2; 10 µM) was applied while recording mIPSCs. Following CB1R agonist application, mIPSC frequency was reduced as anticipated by canonical CB1R activation. However, this reduction was attenuated in MSNs from $ABHD6^{NAc\ KO}$ mice (Fig. 4h). In contrast, no significant difference in mIPSC amplitude following WIN55,212-2 application was observed (Fig. 4i). The amplitude of evoked IPSCs was attenuated to a similar extent in the presence of WIN55,212-2 (Fig. 4j), suggesting similar functional engagement of presynaptic inhibition of GABAergic input to NAc MSNs by exogenous CB1R stimulation. These data suggest that although *Cnr1* expression was reduced in the NAc of $ABHD6^{NAc\ KO}$ mice (Fig. 1d), the capacity for CB1R signalling to attenuate inhibitory input onto NAc MSNs was not impaired. In the presence of CB1R inverse agonist AM251 (2 µM), both mIPSC frequency and amplitude were significantly reduced in MSNs of $ABHD6^{NAc\ KO}$ mice (Fig. 4k–l).

Reductions in m/sIPSC frequency in NAc MSNs from $ABHD6^{NAc\ KO}$ mice (Fig. 4b, d) are consistent with increased presynaptic inhibition of GABAergic release probability that may be mediated by enhanced 2-AG/CB1R signalling following ABHD6 invalidation. However, as mIPSC frequency was also reduced following AM251 (Fig. 4k), these results may involve presynaptic neuroadaptations that persist in the absence of CB1R signalling. Changes in mIPSC amplitude (Fig. 4c) are additionally suggestive of postsynaptic neuroadaptations that may further attenuate inhibitory transmission to NAc MSNs, and indicate there was no homoeostatic compensation to the reduced mIPSC frequency in NAc MSNs from $ABHD6^{NAc\ KO}$ mice[67,68]. Together, these results indicate NAc neuronal ABHD6 loss-of-function reduces basal inhibitory, but not excitatory, transmission to NAc MSNs.

Ventral tegmental area neuronal ABHD6 loss-of-function does not impact body weight gain and reduces locomotor activity on a high-fat diet

Abhd6 mRNA expression within the ventral tegmental area (VTA) was assessed with fluorescent in situ hybridization (Fig. 5a). Expression of *Abhd6* was observed both in *Th*-expressing (*Th*+) and non-*Th*-expressing (*Th*-) cells, consistent with recent RNA-seq results[51,55]. To explore the functional role of neuronal ABHD6 loss-of-function within the VTA, synapsin-promotor GFP (AAV-hSyn-GFP) or Cre recombinase AAVs (AAV-hSyn-Cre) were bilaterally injected into the VTA of adult male $Abhd6^{lox/lox}$ mice to generate $ABHD6^{VTA\ GFP}$ and $ABHD6^{VTA\ KO}$ mice (Fig. 5b). *Abhd6* expression was significantly reduced in $ABHD6^{VTA\ KO}$ mice (Fig. 5c). Body weight gain was not significantly impacted by VTA neuronal ABHD6 loss-of-function over a 6-week period on standard chow diet (Fig. 5d), while a modest but significant increase in food intake was observed in $ABHD6^{VTA\ KO}$ mice (Fig. 5e, Supplementary Fig. 4a, b) without a change in feed efficiency (Fig. 5f). There were no differences in energy expenditure (Supplementary Fig. 4e, f), and a trend toward reduced RER was observed in $ABHD6^{VTA\ KO}$ mice during the dark cycle (Fig. 5g, h), suggesting increased fat utilization. In contrast to the locomotor phenotype observed in $ABHD6^{NAc\ KO}$ mice, no differences in locomotion were observed in $ABHD6^{VTA\ KO}$ mice on the chow diet (Fig. 5i, j).

No differences in body-weight gain (Fig. 5k), body composition (Fig. 5l), food intake (Supplementary Fig. 4g), or feed efficiency (Supplementary Fig. 4h) were observed in $ABHD6^{VTA\ KO}$ mice on HFD. However, in contrast to NAc neuronal ABHD6 loss-of-function which resulted in increased locomotor activity, mice with VTA neuronal ABHD6 loss-of-function exhibited reduced spontaneous locomotor activity on HFD (Fig. 5m), with significantly attenuated locomotor activity during the light cycle (Fig. 5n). No differences in energy expenditure or RER were observed in $ABHD6^{VTA\ KO}$ mice on HFD (Supplementary Fig. 4i–m).

Ventral tegmental area dopamine neuron ABHD6 loss-of-function enhances sucrose-motivated behaviour

As the VTA is functionally implicated in control of mood and social behaviour, we examined whether VTA neuronal ABHD6 loss-of-function may impact anxiety-like behaviour and sociability. No significant differences were observed in the open field test, elevated plus maze test, or 3-chamber social interaction test (Fig. 6a–e, Supplementary Fig. 5a–d). While 2-AG signalling can impact emotional behaviour[69], NAc and VTA findings are consistent with the lack of anxiodepressive-like phenotypes in whole-body ABHD6 knockout mice[70], and are in agreement with findings from MAGL inhibition studies showing that augmented 2-AG signalling fails to impact emotional, social, or anxiety-like behaviour under basal conditions[37,71,72].

Given evidence demonstrating 2-AG signalling within the VTA impacts DA neuron activity and feeding[20,24], we examined the impact of VTA neuronal ABHD6 loss-of-function on sucrose-motivated behaviour using a progressive-ratio operant paradigm (Fig. 6f). $ABHD6^{VTA\ KO}$ mice had similar operant responding in sated conditions (Fig. 6g), however, mesoaccumbens DA responses are known to be modulated by physiological states[73,74]. Considering the activity-dependent "on-demand" nature of 2-AG synthesis and release from DA neurons[18,20,22,23],

https://doi.org/10.1038/s41467-024-54819-5

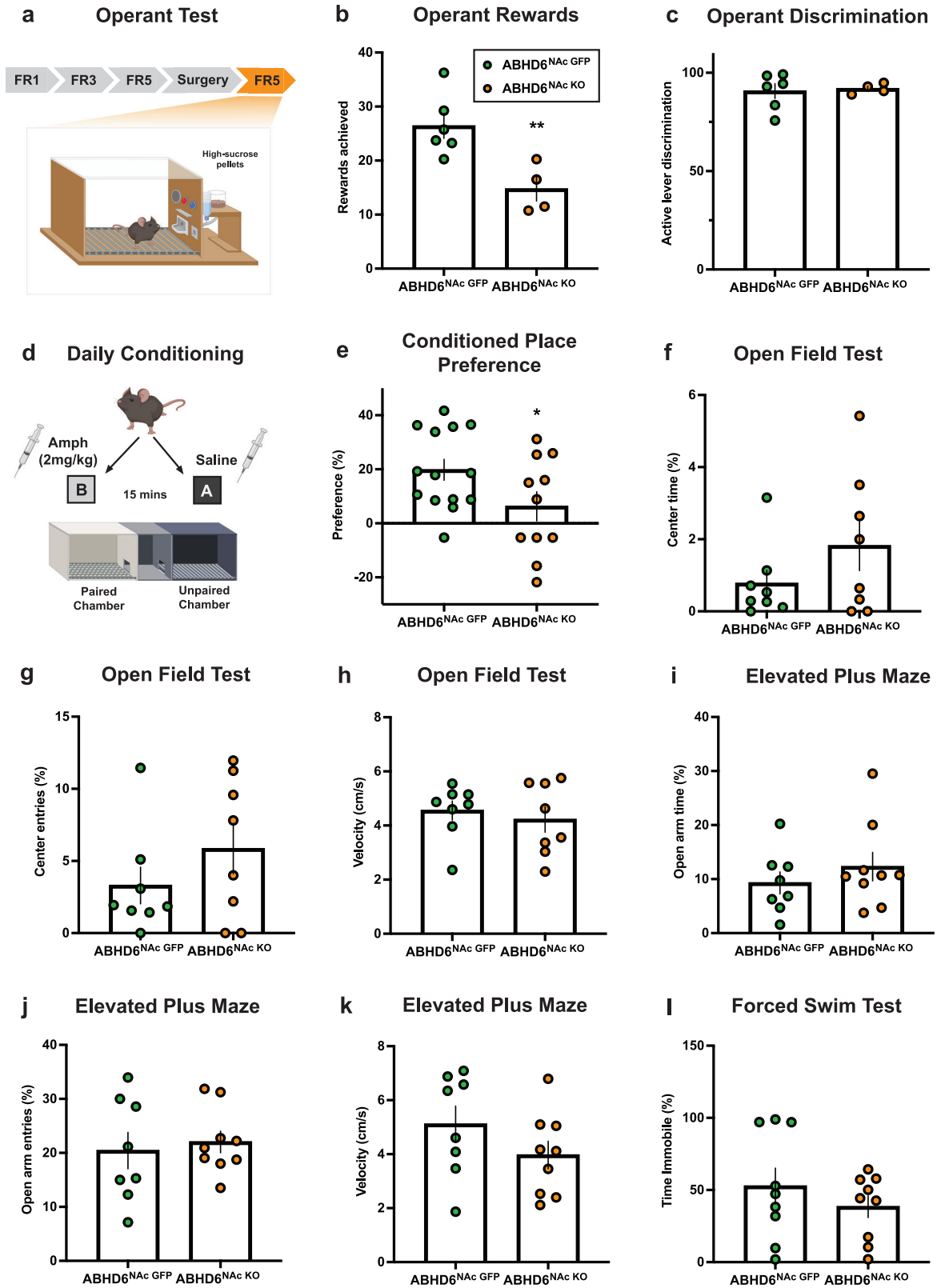

and that food-restriction potentiates DA neuron activity and NAc DA[73], we repeated operant testing after subjecting mice to a 22 hr fast period. While fasting resulted in increased response across mice as expected (Fig. 6g), the magnitude of the increase did not differ between groups (Fig. 6h, i).

The VTA is composed of heterogenous cell types associated with diverse and sometimes opposing reward- and aversion-related functions[75]. Given that *Abhd6* mRNA is expressed within both *Th*+ and *Th*- cells of the VTA (Fig. 5a), it is possible that pan-neuronal deletion of ABHD6 may target 2-AG signalling within GABAergic interneurons[76–78] that may oppose the functional impact of DA neuron 2-AG signalling to inhibitory CB1R inputs that are associated with disinhibition of DA neuron activity and reward[16–20]. To investigate this possibility, we targeted ABHD6 in DA neurons by bilaterally injecting

Fig. 2 | Nucleus accumbens neuronal ABHD6 loss-of-function inhibits the rewarding effects of sucrose and cue-conditioned reward without impacting anxiety- and despair-like behaviour. a Schematic of operant conditioning apparatus. FR, fixed ratio (reinforcement schedule) Created in BioRender. Lau, D. (2023) https://biorender.com/t32u518. **b** Mean operant rewards ($ABHD6^{NAc\ GFP}$: n = 6, $ABHD6^{NAc\ KO}$: n = 4, P = 0.0088). **c** Active lever discrimination ($ABHD6^{NAc\ GFP}$: n = 6, $ABHD6^{NAc\ KO}$: n = 4, P = 0.8118). **d** Schematic of amphetamine place preference conditioning protocol. Created in BioRender. Lau, D. (2023) BioRender.com/x63f624. **e** Amphetamine conditioned place preference data ($ABHD6^{NAc\ GFP}$: n = 14, $ABHD6^{NAc\ KO}$: n = 11, P = 0.0488). **f** Proportion of time in centre of the open field ($ABHD6^{NAc\ GFP}$: n = 8, $ABHD6^{NAc\ KO}$: n = 8, P = 0.2026). **g** Proportion of entries to centre area of open field ($ABHD6^{NAc\ GFP}$: n = 8, $ABHD6^{NAc\ KO}$: n = 8, P = 0.2571). **h** Velocity in the open field apparatus ($ABHD6^{NAc\ GFP}$: n = 8, $ABHD6^{NAc\ KO}$: n = 8, P = 0.5828). **i** Proportion of time spent in the open arms of the elevated-plus maze ($ABHD6^{NAc\ GFP}$: n = 8, $ABHD6^{NAc\ KO}$: n = 9, P = 0.3893). **j** Proportion of entries into open arms of the elevated-plus maze ($ABHD6^{NAc\ GFP}$: n = 8, $ABHD6^{NAc\ KO}$: n = 9, P = 0.6808). **k** Velocity in the elevated-plus maze ($ABHD6^{NAc\ GFP}$: n = 8, $ABHD6^{NAc\ KO}$: n = 9, P = 0.1883). **l** Proportion of time spent immobile in the Porsolt forced swim task ($ABHD6^{NAc\ GFP}$: n = 9, $ABHD6^{NAc\ KO}$: n = 9, P = 0.3415). Data represented as mean ± SEM; *p < 0.05, **p < 0.01. Unpaired two-sided t-test (b-c, e-l). Additional details on statistical tests are available in Supplementary Information. Source data are provided as a Source Data file.

TH-promotor AAV expressing GFP (AAV-Th-GFP) or Cre recombinase (AAV-Th-Cre) to the VTA of adult male *Abhd6*$^{lox/lox}$ mice to generate $ABDH6^{TH\ GFP}$ and $ABHD6^{TH\ KO}$ mice (Fig. 6k). While operant responding was not altered between $ABHD6^{TH\ GFP}$ and $ABHD6^{TH\ KO}$ mice in the sated state, an increased magnitude of change in responding was observed following a 22-hr fast in $ABHD6^{TH\ KO}$ mice (Fig. 6l), as indicated by both an increase in rewards achieved and active lever responses in the fasted state (Fig. 6m, n). Together, these results suggest ABHD6 within VTA DA neurons positively regulates food-directed behaviour in an energy state-dependent manner and implicates functionally oppositional roles of 2-AG signalling from presynaptic (VTA DA) and postsynaptic (NAc MSN) neurons within the mesoaccumbens circuitry to modulate effortful behaviour for food rewards. These findings are consistent with a recent report showing that 2-AG mobilization specifically from VTA DA neurons is crucial for cue-oriented motivated behaviour[19].

Central ABHD6 pharmacological inhibition prevents diet-induced obesity

We next examined whether sustained central pharmacological ABHD6 inhibition may similarly prevent diet-induced obesity in WT mice. Adult male mice on a HFD were subcutaneously implanted with minipumps for chronic intracerebroventricular infusions of either vehicle or the ABHD6-specific inhibitor WWL70[79] on HFD. WWL70-treated mice exhibited reduced body weight gain on HFD (Fig. 7a, b). WWL70 reduced food intake and increased energy expenditure on HFD (Fig. 7c–f). RER was reduced in WWL70-treated mice, suggesting increased fat utilization (Fig. 7g). Similar to $ABHD6^{VTA\ KO}$ mice, a trend towards reduced dark cycle RER and significantly reduced light cycle spontaneous locomotor activity were observed in WWL70-treated mice (Fig. 7g–j). Central ABHD6 inhibition did not alter anxiety-like behaviour (Fig. 7k–l).

Discussion

Increasing CB1R signalling has been classically associated with promoting energy accumulation. By contrast, these results indicate, to our knowledge, the first example of targeted central enhancement of endocannabinoid tone to markedly lower body weight. NAc neuronal ABDH6 deletion leads to a potent catabolic phenotype, a finding consistent with the reduced body weight of mice with whole-body and peripheral ABHD6 knockout[54,70,80]. Results also reveal the capacity of NAc neuronal ABHD6 to modulate reward-directed and DA-dependent behaviour without affecting mood and emotional states that have been well-attributed to some pharmacological CB1R interventions[81]. In contrast, neuronal ABDH6 loss-of-function in the VTA produced modest anabolic effects yet failed to affect motivation for food. On the other hand, selective knockout of ABHD6 in DA neurons of the VTA produced stimulated sucrose-directed behaviour, in agreement with the well-known effects of DA signalling and CB1R stimulation to augment food-directed behaviour. Consistent with the powerful NAc intervention results, chronic central pharmacological ABHD6 inhibition also conferred protection against diet-induced obesity. Together, these findings uncover unique mechanisms for the control of body weight and physical activity via central and mesoaccumbens ABHD6 regulation.

Invalidation of NAc neuronal ABHD6 was additionally associated with neurophysiological adaptations including reduced basal synaptic inhibitory, but not excitatory, transmission onto NAc MSNs. The specific differences may be explained by greater abundance and/or sensitivity for CB1R endocannabinoid signalling on GABAergic synapses[32,82,83], and the possibility that the unique subcellular localization of postsynaptic ABHD6 within NAc neurons may regulate degradation of distinct 2-AG signalling pools in a non-redundant manner to presynaptic MAGL[4]. As a proof-of-principle example of how subcellular ABHD6 expression patterns may be coupled to pathway-specific control of unique 2-AG signalling pools, recent results have demonstrated stimuli-dependent control of metabotropic-, but not ionotropic-, derived 2-AG degradation by ABHD6 within Neuro2a cells[84]. The potential for synapse- and/or pathway-specific regulation of 2-AG pools by ABHD6 is an attractive hypothesis to distinguish the impact of NAc neuronal ABHD6 loss-of-function from the impact of NAc CB1R signalling generally. Moreover, our findings are in agreement with the growing appreciation for cellular- and subcellular-specificity of 2-AG/CB1R signalling to mediate diverse, and occasionally functionally opposing, effects on physiology and behaviour[85].

Control of canonical 2-AG/CB1R signalling represents the most characterized mechanism of ABHD6 action within the brain. However, other mechanisms of ABHD6 action and 2-AG signalling have been previously noted. For example, ABHD6 has been demonstrated to modulate synaptic signalling and plasticity independently of enzymatic 2-AG degradation via negative regulation of postsynaptic AMPA receptor trafficking[86–88]. However, no differences in EPSCs in NAc MSNs from $ABHD6^{NAc\ KO}$ mice were observed, arguing against involvement of ABHD6-mediated control of AMPA receptor trafficking. Additionally, CB1R-independent positive allosteric modulation of $GABA_A$ receptor function by 2-AG has been indicated from heterologous expression studies and pharmacological experiments in CB1R-knockout mice[89,90]. However, our electrophysiological results indicate inhibitory drive is reduced, rather than increased as would be anticipated by increasing 2-AG tone. Thus, while our data cannot rule out the possible contribution of non-canonical actions of 2-AG and ABHD6, our findings are broadly consistent with neuronal ABHD6 controlling presynaptic CB1R signalling via augmented 2-AG within the NAc. Chronic cannabis usage is also paradoxically associated with reduced BMI[91–93], an effect that is not driven by reduced energy intake[94–96]. A mechanistic basis for this phenomenon remains unclear. However, it has been hypothesized that compensatory downregulation of CB1R may be involved[97].

Our results demonstrated an anorectic impact of central ABHD6 pharmacological inhibition in wildtype mice on a HFD. This finding is consistent with modest reductions of food intake in whole-body ABHD6 knockout mice on HFD[70]. Because food intake is unchanged following peripherally-restricted ABHD6 knockdown by antisense oligonucleotide treatment[80], our findings suggest lower food intake from whole-body ABHD6 knockout is mediated by loss of ABHD6 function within the brain. A trend towards reduced HFD food intake was

https://doi.org/10.1038/s41467-024-54819-5

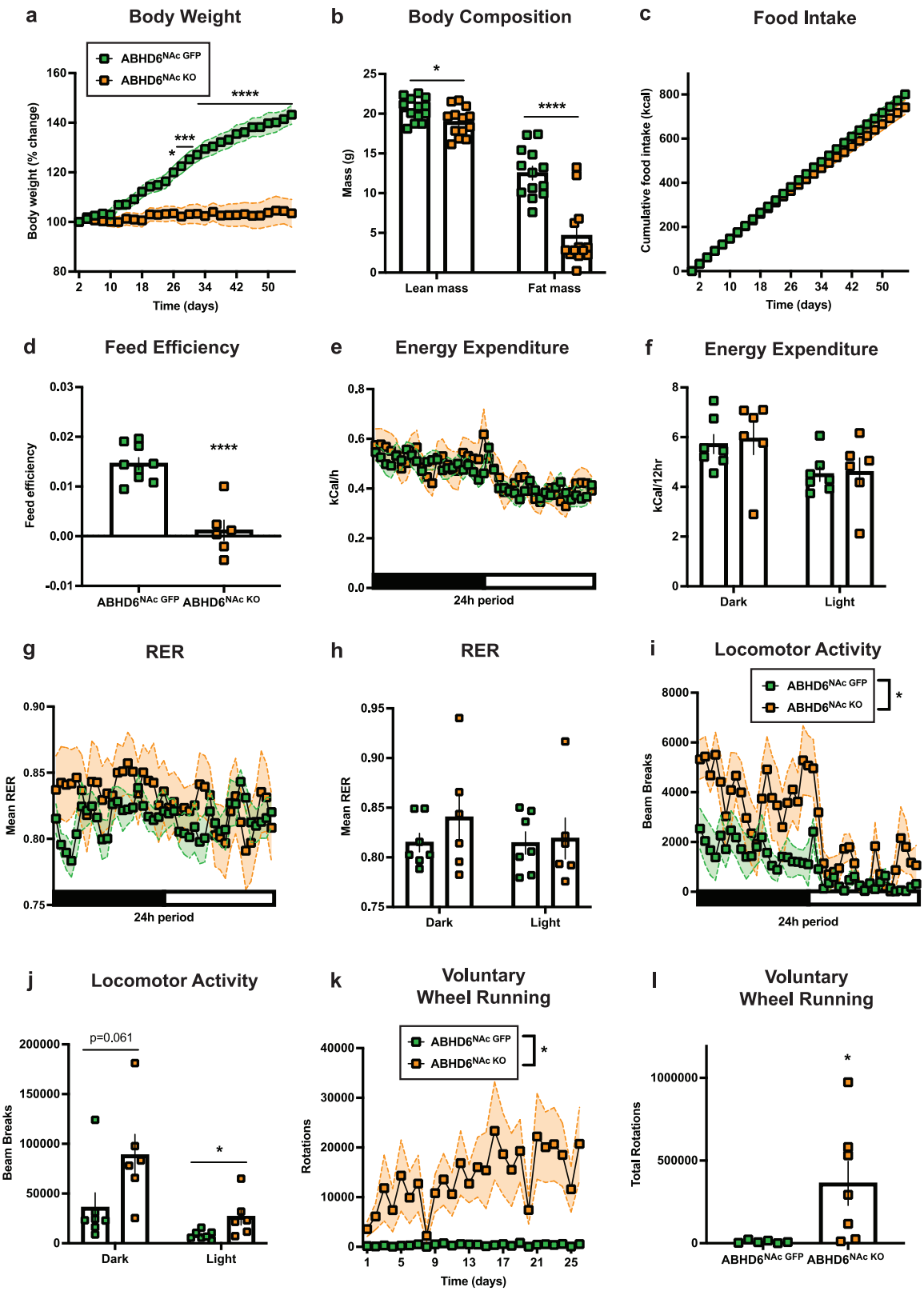

observed in ABHD6$^{NAc\ KO}$ mice. These data stand in contrast to previously described orexigenic effects of 2-AG/CB1R signalling, including within the NAc and limbic forebrain, to stimulate food intake[98,99]. Cell-type specific CB1R-knockout experiments of Bellocchio and colleagues revealed that hyperphagia evoked by CB1R agonism or refeeding following a fast requires CB1R signalling in cortical glutamatergic neurons[100]. Conversely, ventral striatal CB1R expressed in GABAergic neurons mediate an opposing, anorectic effect[100]. Thus, while the overarching impact of CB1R signalling in the NAc promotes food-intake, synapse-specific control of NAc CB1R signalling exerts bimodal impacts on feeding, with activation of CB1R present on GABAergic terminals in the NAc (reducing NAc inhibition) reducing food intake, and activation of CB1R present on glutamatergic terminals in the NAc (reducing NAc excitation) increasing food intake. In line with these

Fig. 3 | Nucleus accumbens neuronal ABHD6 deletion prevents diet-induced obesity and associated spontaneous and voluntary inactivity. a Body weight on HFD (ABHD6$^{NAc\ GFP}$: n = 9, ABHD6$^{NAc\ KO}$: n = 6, two-way ANOVA interaction P < 0.0001). **b** Lean (ABHD6$^{NAc\ GFP}$: n = 13, ABHD6$^{NAc\ KO}$: n = 13, P = 0.0219) and fat mass (ABHD6$^{NAc\ GFP}$: n = 13, ABHD6$^{NAc\ KO}$: n = 13, P < 0.0001). **c** Free-feeding HFD intake (ABHD6$^{NAc\ GFP}$: n = 9, ABHD6$^{NAc\ KO}$: n = 6, two-way ANOVA interaction P < 0.0001). **d** Feed efficiency (ABHD6$^{NAc\ GFP}$: n = 9, ABHD6$^{NAc\ KO}$: n = 6, P < 0.0001). **e** Energy expenditure over time (indirect calorimetry; ABHD6$^{NAc\ GFP}$: n = 7, ABHD6$^{NAc\ KO}$: n = 6, two-way ANOVA interaction P = 0.0059). **f** Energy expenditure during dark (ABHD6$^{NAc\ GFP}$: n = 7, ABHD6$^{NAc\ KO}$: n = 6, P = 0.7652) or light cycle (ABHD6$^{NAc\ GFP}$: n = 7, ABHD6$^{NAc\ KO}$: n = 6, P = 0.8908). **g** Respiratory exchange ratio (RER, indirect calorimetry; ABHD6$^{NAc\ GFP}$: n = 7, ABHD6$^{NAc\ KO}$: n = 6, two-way ANOVA interaction P = 0.0283). **h** Mean RER in (g) during dark (ABHD6$^{NAc\ GFP}$: n = 7, ABHD6$^{NAc\ KO}$: n = 6, P = 0.3110) or light cycle (ABHD6$^{NAc\ GFP}$: n = 7, ABHD6$^{NAc\ KO}$: n = 6, P = 0.8444). **i** Locomotor activity (ABHD6$^{NAc\ GFP}$: n = 7, ABHD6$^{NAc\ KO}$: n = 6, two-way ANOVA group main effect P = 0.0310). **j** Locomotor activity in (**i**) during dark (ABHD6$^{NAc\ GFP}$: n = 7, ABHD6$^{NAc\ KO}$: n = 6, P = 0.0610) or light cycle (ABHD6$^{NAc\ GFP}$: n = 7, ABHD6$^{NAc\ KO}$: n = 6, P = 0.0407). **k** Voluntary wheel-running over 26 days (ABHD6$^{NAc\ GFP}$: n = 6, ABHD6$^{NAc\ KO}$: n = 7, two-way ANOVA group main effect P = 0.0338). **l** Cumulative wheel-running from (**k**) (ABHD6$^{NAc\ GFP}$: n = 6, ABHD6$^{NAc\ KO}$: n = 7, P = 0.0338). Data represented as mean ± SEM; *p < 0.05, **p < 0.01, ***p < 0.001, ****p < 0.0001. Unpaired two-sided t-test (**b**, **d**, **f**, **h**, **j**, **l**), two-way ANOVA group x time interaction with Sidak's post hoc correction (**a**, **c**), two-way ANOVA group x time interaction (**e**, **g**), two-way ANOVA group main effect (i, k). Additional details on statistical tests are available in Supplementary Information. Source data are provided as a Source Data file.

findings, pharmacological studies have consistently demonstrated GABA receptor agonism (increasing NAc inhibition) in the NAc shell increases feeding[101–103].

Decreases in NAc shell MSN activity are associated with increased food consumption[104–106], via a NAc shell dopamine D1 receptor MSN circuit projecting to the lateral hypothalamus[107,108]. Our electrophysiological findings demonstrated reduced inhibitory input onto NAc MSNs, as indicated by reduced s/mIPSC frequency and amplitude, consistent with reduced NAc inhibition and an impact on CB1R expressed on GABAergic, not glutamatergic, synapses to NAc MSNs. Thus, the absence of an orexigenic phenotype observed in ABHD6$^{NAc\ KO}$ mice is in agreement with the functional role of CB1R signalling on glutamatergic, not GABAergic, neurons to promote feeding[100]. In contrast, a modest increase in cumulative food-intake on a standard chow diet was observed following VTA neuronal ABHD6 loss-of-function, similar to the impact of ABHD6 knockout from VMH neurons[53]. However, such changes were absent during fasting-induced chow refeeding and chronic HFD. It is possible that other physiological systems mediating adaptation to metabolic challenges overrode the ability to detect differences in orexigenic drive on chow diet. Collectively, these findings underscore site-specific impacts of central and mesoaccumbal neuronal ABHD6 to control food intake in a diet- and energy state-dependent manner.

Cannabinoid-induced impairments in motor performance mediated by stimulation of CB1R signalling are well-known, including general inhibition of locomotion, and induction of immobility and catalepsy[16,49,109–111]. Pharmacological NAc cannabinoid receptor stimulation is sufficient to induce catalepsy[112], and systemic MAGL inhibition or 2-AG treatment tends to attenuate locomotor activity[89,113–115]. In a similar manner, VTA neuronal ABHD6 invalidation resulted in reduced locomotor activity on HFD. In contrast, NAc neuronal loss-of-function resulted in robust increases in spontaneous locomotion and voluntary wheel-running during HFD. These findings match previous studies demonstrating that both whole-body ABHD6-knockout[70] and peripherally-restricted antisense oligonucleotide knockdown of ABHD6[80] increase physical activity, with ABHD6-knockout mice additionally exhibiting increased locomotor-activating effects of amphetamine[116]. Central pharmacological ABHD6 inhibition resulted in both catabolic actions to reduce weight gain on HFD (similar to NAc neuronal ABHD6 knockout) and inhibit spontaneous locomotor activity on HFD (similar to VTA neuronal ABHD6 knockout). This suggests that while brain-wide ABHD6 inhibition conferred protection against diet-induced obesity consistent with NAc neuronal ABHD6 invalidation, it partially recapitulated a mixture of phenotypes observed from NAc and VTA neuronal ABHD6 deletion on HFD. Collectively, findings suggest that ABHD6 regulates movement via multiple peripheral and central systems, with neuronal NAc and VTA ABHD6 exerting opposing effects on physical activity on HFD.

The reduced basal inhibitory synaptic transmission onto NAc MSNs coupled with increased spontaneous locomotion in ABHD6$^{NAc\ KO}$ mice is consistent with pharmacological studies demonstrating intra-NAc GABA receptor pharmacological antagonism elevates locomotor activity[117,118]. Within the dorsal striatum, CB1R is prominently expressed within MSNs to mediate important behavioural and synaptic functions, including modulation of MSN-to-MSN lateral inhibition[32,40,45,119–121]. In contrast, CB1R is not expressed within MSNs of the murine NAc (ventral striatum), with GABAergic fast-spiking interneurons (FSIs) representing the exclusive cellular source of local CB1R expression within the NAc[39,41,42,52]. While parvalbumin-expressing NAc FSIs comprise a small minority of NAc cells, they mediate powerful feed-forward inhibition onto NAc MSNs[122]. This FSI-to-MSN feed-forward inhibition is negatively modulated by CB1R signalling on FSI terminals to MSNs[38–43]. NAc FSIs are additionally themselves capable of regulating synaptic transmission onto their pre-synaptic cortical and thalamic CB1R-expressing glutamatergic inputs via endocannabinoid synthesis/release, however these effects are most likely mediated by anandamide rather than 2-AG[123,124]. Dorsal striatal FSIs may be dispensable for the expression of normal locomotion[125], however numerous studies have linked striatal FSI activity to control of movement[126–129]. CB1R-expressing FSIs within the NAc represent a subset of NAc FSIs[39]. Suggesting a function in locomotion, pharmacological blockade of calcium-permeable AMPA receptors expressed on NAc parvalbumin neurons (a manipulation that should attenuate NAc FSI-to-MSN feed-forward inhibition) enhances physical activity[123]. By contrast, genetic *Cnr1* knockout experiments suggest that CB1R signalling within either direct- or indirect-pathway dorsal striatal MSNs is dispensable for basal locomotion[121]. Although our data cannot directly address whether altered basal inhibitory transmission onto NAc MSNs is mechanistically causal to enhanced spontaneous locomotion, it is tempting to speculate reduced NAc FSI-to-MSN feed-forward inhibition in ABHD6$^{NAc\ KO}$ mice may represent a candidate mechanism to disinhibit locomotion, potentially via MSN outputs controlling the mesencephalic locomotor region, an area critical for spontaneous movement[130–132].

NAc dopamine mediates a vital role in the control of locomotion and motivated behaviour[133,134]. Emphasizing this, effort-related choice and behavioural economic paradigms have demonstrated that manipulations of NAc dopamine function powerfully alter cost-benefit computations underlying motivated behaviour[135–137], which can occur orthogonally to changes in intake[138–140]. Numerous investigations over the past two decades have delineated a crucial role for modulation of mesoaccumbens DA function by endocannabinoid signalling to control motivated behaviour[9–12,61]. Intra-VTA CB1R signalling generally promotes elevated NAc DA release via disinhibition of VTA dopamine neurons[16–18], potentially mediated by signalling-specific phosphorylation of MAPK (p-ERK1/2) downstream from CB1R activation[141]. In line with the impact of NAc dopamine to promote reward-seeking, effortful behaviour[133], CB1R agonism generally promotes increased motivation in operant instrumental behaviour tasks[20,142–144], while CB1R antagonism or genetic deletion generally exerts an opposing effect of reduced operant responding[26,143–149]. Consistent with this, inhibition of 2-AG degradation via pharmacological MAGL antagonism enhances motivation during instrumental operant behaviour for food rewards in a

https://doi.org/10.1038/s41467-024-54819-5

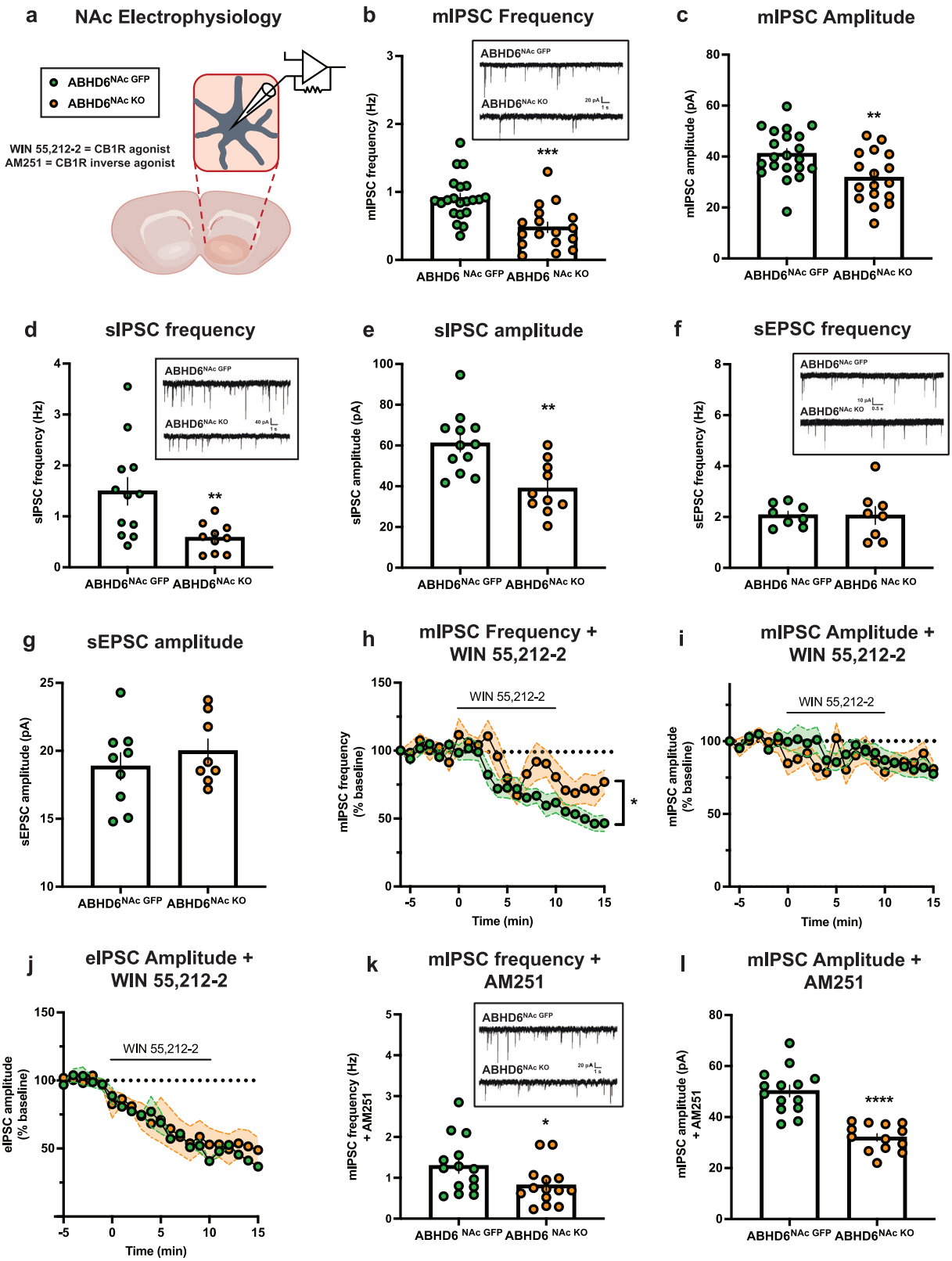

CB1R-dependent manner[20,29]. Our results indicate pan-neuronal deletion of ABHD6 in the VTA did not impact food reward-directed instrumental operant behaviour. However, consistent with evidence linking endocannabinoid modulation of VTA DA neuronal activity with food- motivated behaviour[11,12,19,61], targeting ABHD6 specifically from VTA DA neurons enhanced effortful behaviour in the fasted state to a greater extent than controls. These findings are concordant with recent evidence demonstrating that the positive control of motivated behaviour for palatable food relies upon 2-AG signalling originating specifically from VTA DA neurons[19]. In contrast to VTA results, deletion of ABHD6 from NAc neurons restrained food-reward directed operant behaviour and attenuated amphetamine place preference. Blunted reward-related behaviour in ABHD6$^{NAc\ KO}$ mice is consistent with evidence that pharmacological CB1R agonism or MAGL inhibition

Fig. 4 | ABHD6 loss-of-function attenuates inhibitory input onto nucleus accumbens medium spiny neurons. a Schematic of whole-cell patch-clamp electrophysiology of NAc MSNs. Created in BioRender. Lau, D. (2023) BioRender.com/s42q889. **b** mIPSC frequency (ABHD6$^{NAc\ GFP}$: n = 21, ABHD6$^{NAc\ KO}$: n = 17, P = 0.0002). The inset illustrates representative mIPSC traces. **c** mIPSC amplitude (ABHD6$^{NAc\ GFP}$: n = 21, ABHD6$^{NAc\ KO}$: n = 17, P = 0.0053). **d** sIPSC frequency (ABHD6$^{NAc\ GFP}$: n = 12, ABHD6$^{NAc\ KO}$: n = 10, P = 0.0081). The inset illustrates representative sIPSC traces. **e** sIPSC amplitude (ABHD6$^{NAc\ GFP}$: n = 12, ABHD6$^{NAc\ KO}$: n = 10, P = 0.0014). **f** sEPSC frequency (ABHD6$^{NAc\ GFP}$: n = 8, ABHD6$^{NAc\ KO}$: n = 8, P = 0.9725). Inset illustrates representative sEPSC traces. **g** sEPSC amplitude (ABHD6$^{NAc\ GFP}$: n = 9, ABHD6$^{NAc\ KO}$: n = 8, P = 0.4198). **h** mIPSC frequency following application of CB1R agonist (WIN 55,212-2) (ABHD6$^{NAc\ GFP}$: n = 10, ABHD6$^{NAc\ KO}$: n = 8, two-way ANOVA group main effect P = 0.0497). **i** mIPSC amplitude following application of CB1R agonist (WIN 55,212-2) (ABHD6$^{NAc\ GFP}$: n = 10, ABHD6$^{NAc\ KO}$: n = 8, two-way ANOVA interaction P = 0.2261). **j** eIPSC amplitude following application of CB1R agonist (WIN 55,212-2) (ABHD6$^{NAc\ GFP}$: n = 2, ABHD6$^{NAc\ KO}$: n = 3, two-way ANOVA interaction P = 0.9757). **k** mIPSC frequency following application of CB1R inverse agonist (AM251) (ABHD6$^{NAc\ GFP}$: n = 14, ABHD6$^{NAc\ KO}$: n = 14, P = 0.0446). Inset illustrates representative mIPSC traces following AM251 application. **l** mIPSC amplitude following application of CB1R inverse agonist (AM251) (ABHD6$^{NAc\ GFP}$: n = 14, ABHD6$^{NAc\ KO}$: n = 13, P < 0.0001). Data represented as mean, with error bars/shaded areas ± SEM; *p < 0.05, **p < 0.01, ***p < 0.001, ****p < 0.0001. Unpaired two-sided t-test (**b**–**g**, **k**, **l**), two-way ANOVA group x time interaction (**i**, **j**), two-way ANOVA group main effect (**h**). Additional details on statistical tests are available in Supplementary Information. Source data are provided as a Source Data file.

attenuate NAc cholinergic interneuron optical stimulation-evoked DA release[150], CB1R signalling on medial-prefrontal afferents to the NAc restrains motivated behaviour[150], intra-accumbal CB1R pharmacological inhibition induces place preference[151], and exogenous CB1R agonism in the NAc posterior shell promotes aversion behaviours[152]. In this manner, the opposing impacts on reward-seeking of augmented 2-AG/CB1R signalling between presynaptic VTA DA neurons[20] and postsynaptic MSNs[150] of the mesoaccumbens circuitry are consistent with our results, and support the notion that the effects of mesoaccumbal CB1R stimulation to enhance reward-directed behaviour are mediated via modulation of presynaptic (VTA) DA neuron activity[27], rather than postsynaptic accumbal neurons.

Limitations

While our viral approach invalidated ABHD6 from NAc neurons, it did not specifically target core or shell subregions known to have heterogenous functional properties[153]. Additionally, our pan-neuronal viral approach did not specifically target MSN cell-types within the NAc, which may be differentially modulated by endocannabinoid signalling[154–156]. Our results do not address the possible role of ABHD6 to impact non-canonical 2-AG signalling actions, including mesoaccumbal CB2R[157,158], cell-autonomous signalling in midbrain DA neurons[159], or other impacts of ABHD6 to control glycerophos pholipid[80] and bis(monoacylcero)phosphate[160] metabolism. Our findings cannot rule out the possibility that altered 2-AG metabolism via ABHD6 blockade/invalidation may indirectly exert impacts on additional lipid signalling networks given the integrated nature of 2-AG within other lipid signalling pathways[161,162]. Our electrophysiological experiments with WIN55,212-2 were performed in the absence of BSA, which may well underestimate the magnitude of CB1R stimulation[163,164]. Additionally, it is unclear if differences we observed in response to WIN are due to CB1R activation as the 10 μM dose of WIN applied may activate non-CB1R targets[165,166]. There is a wealth of evidence indicating neuronal ABHD6 controls canonical endocannabinoid signalling[3,6]; however, the potential role of ABHD6 in glial-derived synthesis or termination of 2-AG signalling[167,168] and glial CB1R signalling[65,169,170] represents an interesting area for future investigation.

Methods

Animals

All experimental procedures were approved by the CRCHUM animal care committee (AN13009SFs, CM17019SFs) and conducted in accordance with Canadian Council on Animal Care guidelines. *Abhd6*$^{lox/lox}$ mice were generated and backcrossed for at least 8 generations on a C57BL/6N background[54] and used for all experiments unless otherwise noted. Previous work has established that *Abhd6*$^{lox/lox}$ mice have similar body weight gain and food intake to wild-type mice[54,171]. Adult male mice were used for all experiments. For all metabolic and behavioural experiments, mice were housed in a sterile barrier facility with light (reverse 12 hr light/12 hr dark cycle; lights off at 10AM), humidity (45–55%), and temperature (22 °C) control, with all in vivo testing and animal sacrifices conducted during the dark phase of the light cycle. Animal health and safety were monitored throughout the study by both researchers and animal care staff. Unless otherwise noted, mice had ad libitum access to food and water throughout. Within the homecage, handling tubes were used to mitigate handling stress. For electrophysiological studies, mice were housed under a normal light cycle and sacrificed during the light phase. For in vivo ventral pharmacological experiments, adult male wild-type C57Bl/6NCrl (Charles River) mice were used. For NAc fluorescent in situ hybridization experiments, adult wild-type C57BL/6J (Jackson) mice were used. All mice were sacrificed under isoflurane (5%) anaesthesia except mice receiving cardiac perfusions for RNAscope and immunohistochemical experiments for which sodium pentobarbital (200 mg/kg, IP) was used. A list of key resources is available in the Supplementary Information key resources table (Supplementary Table 1).

Stereotaxic surgeries

NAc stereotaxic surgeries: Adult male *Abhd6*$^{lox/lox}$ mice used for all metabolic and behavioural experiments. For all in vivo NAc experiments, except for the operant testing experiment, mice had NAc targeted surgery at 8–10 weeks of age at the time of surgical procedure and allowed to recover for 2 weeks prior to experiments. Animals were weight-matched between groups. For operant experiments, mice received surgery following successful completion of operant training[172], beginning at approximately 9–10 weeks of age, with surgery around 13 weeks of age. For mice used for NAc ex vivo electrophysiological experiments, male *Abhd6*$^{lox/lox}$ mice received surgery at 6 weeks of age. For all surgeries, mice were anesthetized with isoflurane (1.5% maintenance) and secured in a stereotaxic frame (Kopf), with adeno-associated viral injections via a 33-gauge Neuros 7000 series syringe (Hamilton). Standard stereotaxic surgical techniques were used for all surgeries, and all mice were single-housed following surgery and for experiments. Coordinates for bilateral targeting of the NAc were AP: +1.6, ML: +/−1.1, DV: −4.5; 500 nl/side. For neuron-specific targeting of ABHD6, mice received injections of either AAV2/1.hSynapsin.HI.EGFP.WPRE.bGH (2.5-5.0×10^9 GC/μl, Penn Vector Core) to deliver GFP ("ABHD6$^{NAc\ GFP}$") or AAV2/1.hSynapsin.HI.GFP.-Cre.WPRE.SV40 (2.5-5.0×10^9 GC/μl, Penn Vector Core) to deliver Cre-recombinase ("ABHD6$^{NAc\ KO}$") under the control of the synapsin promotor.

VTA stereotaxic surgeries: Adult male *Abhd6*$^{lox/lox}$ mice used for metabolic and most behavioural experiments (except for operant testing experiment) had surgery at 9–11 weeks of age at the time of the surgical procedure. Animals were weight-matched between groups. For operant experiments, mice received surgery following successful completion of operant training[172] beginning around 10–11 weeks of age, with surgery around 17–18 weeks of age. Stereotaxic surgical procedures were used as described above, with bilateral viral injections targeting the VTA (AP −3.4: ML: +/−0.4, DV: −4.15; 500 nl/side) of an adeno-associated virus. For experiments with pan-neuronal

https://doi.org/10.1038/s41467-024-54819-5

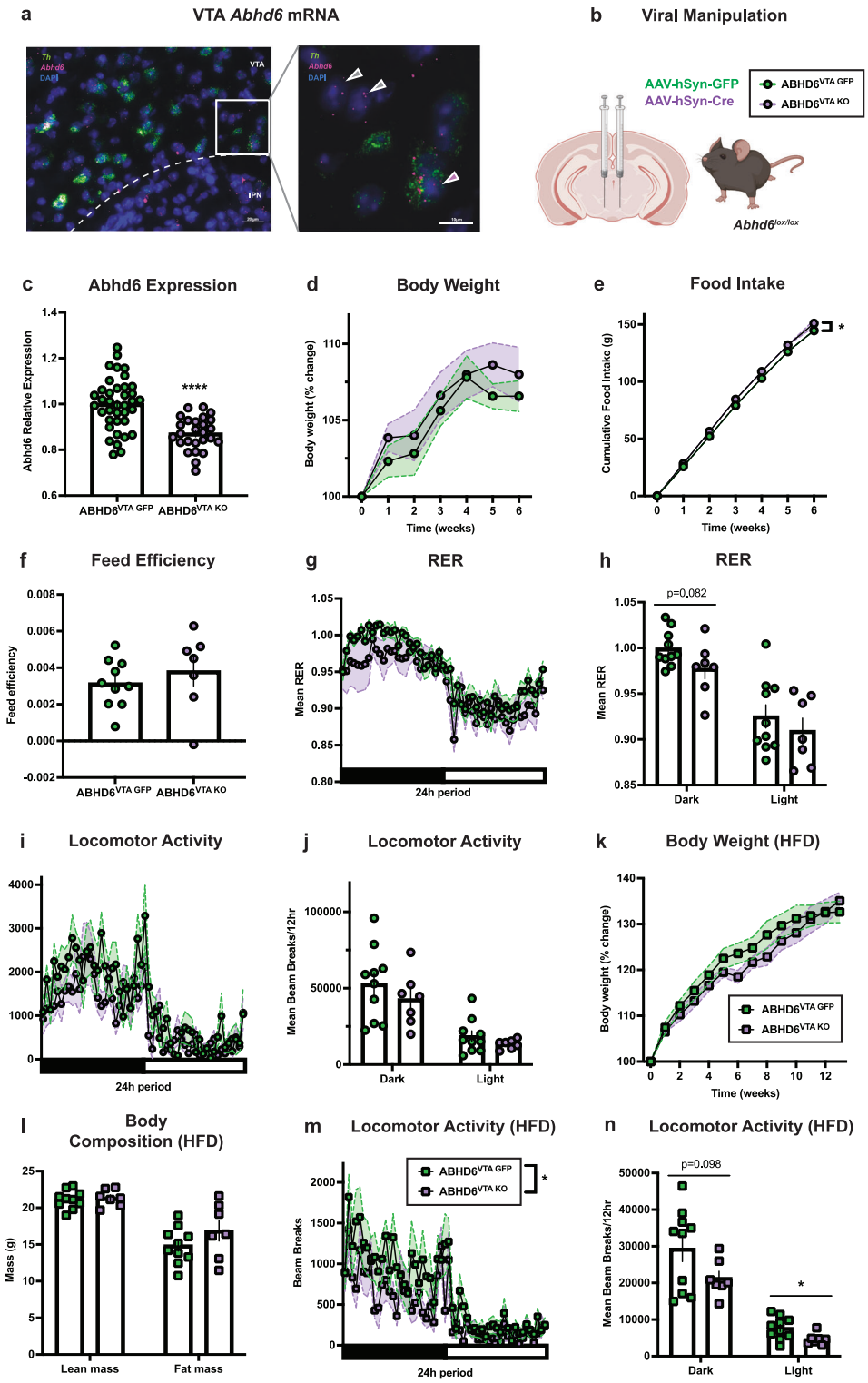

targeting of VTA cells, mice received injections of either AAV2/1.hSynapsin.HI.EGFP.WPRE.bGH (3.876 × 10^{11}GC/mL, Penn Vector Core) to deliver GFP ("ABHD6$^{VTA\ GFP}$") or AAV2/1.hSynapsin.HI.GFP.Cre.WPRE.SV40 (2.8 × 10^{11}GC/mL, Penn Vector Core) to deliver Cre-recombinase ("ABHD6$^{VTA\ KO}$"). For experiments targeting ABHD6 in VTA dopamine neurons[19,173], mice received injections of either AAV9.TH.eGFP.WPRE.rBG (5 × 10^{11}GC/mL, Penn Vector Core) to deliver GFP ("ABHD6$^{TH\ GFP}$") or AAV9.rTH.PI.Cre.SV40 (5 × 10^{11}GC/mL, Penn Vector Core) to deliver Cre recombinase ("ABHD6$^{TH\ KO}$").

Lateral ventricular cannulation surgeries: Adult male wild-type C57Bl/6NCrl mice (Charles River) were used for intracerebroventricular (ICV) injection experiments. A guide cannula targeting the lateral ventricle (AP: −0.5, ML: 1.1, DV: −2.5) was secured to the skull and attached to a 28-day mini osmotic-pump (Alzet, model 2004) delivering the ABHD6 inhibitor WWL70 (Cayman Chemical) in 20% DMSO (Sigma-Aldrich) or vehicle (20% DMSO). WWL70 is a pharmacological inhibitor with high selectivity for ABHD6[79]. The dose of 1.86 µg/day is approximately 135-fold dilution from the systemic dose used

Fig. 5 | Neuronal ABHD6 loss-of-function in the ventral tegmental area fails to affect body weight. a Photomicrograph of VTA showing representative in situ hybridization expression of *Th* (green) and *Abhd6* (red) of 6 experiments from 3 mice. Inset demonstrates VTA *Abhd6* expression within *Th*-expressing (purple arrow) and non-*Th*-expressing (grey arrows) cells. IPN, interpeduncular nucleus. **b** Schematic of viral manipulation. Created in BioRender. Lau, D. (2023) BioRender.com/e70i609. **c** VTA *Abhd6* gene expression (ABHD6$^{VTA\ GFP}$: n = 38, ABHD6$^{VTA\ KO}$: n = 26, P < 0.0001). **d** Body weight (ABHD6$^{VTA\ GFP}$: n = 10, ABHD6$^{VTA\ KO}$: n = 7, two-way ANOVA interaction P = 0.8996). **e** Food intake (ABHD6$^{VTA\ GFP}$: n = 10, ABHD6$^{VTA\ KO}$: n = 7, two-way ANOVA group main effect P = 0.0143). **f** Feed efficiency (ABHD6$^{VTA\ GFP}$: n = 10, ABHD6$^{VTA\ KO}$: n = 7, P = 0.4422). **g** Respiratory exchange ratio (ABHD6$^{VTA\ GFP}$: n = 10, ABHD6$^{VTA\ KO}$: n = 7, two-way ANOVA interaction P = 0.8794). **h** Mean RER in (**g**) during dark (ABHD6$^{VTA\ GFP}$: n = 10, ABHD6$^{VTA\ KO}$: n = 7, P = 0.0818) or light cycle (ABHD6$^{VTA\ GFP}$: n = 10, ABHD6$^{VTA\ KO}$: n = 7, P = 0.4202). **i** Locomotor activity (ABHD6$^{VTA\ GFP}$: n = 10, ABHD6$^{VTA\ KO}$: n = 7, two-way ANOVA interaction P = 0.2223). **j** Locomotor activity in (**i**) during the dark (ABHD6$^{VTA\ GFP}$: n = 10, ABHD6$^{VTA\ KO}$: n = 7, P = 0.3675) or light cycle (ABHD6$^{VTA\ GFP}$: n = 10, ABHD6$^{VTA\ KO}$: n = 7, P = 0.2571). **k** Body weight on HFD (ABHD6$^{VTA\ GFP}$: n = 10, ABHD6$^{VTA\ KO}$: n = 7, two-way ANOVA interaction P = 0.1262). **l** Lean mass (ABHD6$^{VTA\ GFP}$: n = 10, ABHD6$^{VTA\ KO}$: n = 7, P = 0.7274) and fat mass (ABHD6$^{VTA\ GFP}$: n = 10, ABHD6$^{VTA\ KO}$: n = 7, P = 0.1987). **m** Locomotor activity on HFD (ABHD6$^{VTA\ GFP}$: n = 10, ABHD6$^{VTA\ KO}$: n = 7, two-way ANOVA group main effect P = 0.0443). **n** Locomotor activity on HFD in (**m**) during dark (ABHD6$^{VTA\ GFP}$: n = 10, ABHD6$^{VTA\ KO}$: n = 7, P = 0.0976) or light cycle (ABHD6$^{VTA\ GFP}$: n = 10, ABHD6$^{VTA\ KO}$: n = 7, P = 0.0271). Data represented as mean, with error bars/shaded areas ± SEM; *p < 0.05, ****p < 0.0001. Unpaired two-sided t-test (**c**, **f**, **h**, **j**, **l**, **n**), two-way ANOVA group x time interaction (**d**, **g**, **i**, **k**), two-way ANOVA group main effect (**e**, **m**). Additional details on statistical tests are available in Supplementary Information. Source data are provided as a Source Data file.

previously[70] (10 mg/kg, i.p.) and is similar to the dose previously used centrally[53].

Dietary manipulations

Unless otherwise noted, mice were fed on standard chow with *ad libitum* access in the home-cage. For all experiments with high-fat diet, mice were fed on a palm-oil-based saturated high-fat rodent diet with 50% of kcal fat[174,175] (Modified AIN-93G purified rodent diet, Dyets) under ad libitum access. For ABHD6$^{NAc\ GFP}$ and ABHD6$^{NAc\ KO}$ animals, one cohort of animals was used to assess the metabolic, behavioural, and biochemical (RT-qPCR) impact of 8 weeks of feeding on chow and HFD. An additional cohort of animals on chow or HFD was used to assess wheel running on chow or HFD. For ABHD6$^{VTA\ GFP}$ and ABHD6$^{VTA\ KO}$ animals, a single cohort of animals was used to assess metabolic impact of 6 weeks of feeding on chow, followed by 13 weeks on HFD, with a separate cohort of animals used to assess emotion- and social-related behaviour on chow diet.

Fast-refeeding experiments

For ABHD6$^{VTA\ GFP}$ and ABHD6$^{VTA\ KO}$ mice, fast-refeeding response was assessed at 3 weeks following surgery on a chow diet. Baseline hourly feeding was assessed at 0, 1, 2, 3, 4, 6, 8, 12, and 24 hr timepoints beginning at the onset of the dark cycle. At 12 hr (2 hr into the dark cycle), home-cage food was removed, with refeeding responses beginning at 10 hr (onset of the dark cycle) the following day at the same hourly time points with the return of ad libitum access to standard chow diet in home-cage. For VTA operant experiments, mice were also subjected to a 22 hr fast with home-cage chow food removed approximately 1 hr following completion of operant testing on the second last day, for a fast period of 22 hr when mice were tested on the operant paradigm again at the usual time the following day.

Body composition and metabolic phenotyping

Fat and lean mass were assessed using EchoMRI nuclear magnetic resonance apparatus. Indirect calorimetry from the Comprehensive Lab Animal Monitoring System (CLAMS, Columbus Instruments) at 22 °C was used for metabolic phenotyping, with oxygen consumption and carbon dioxide production used to estimate energy expenditure and respiratory exchange ratio. Additionally, spontaneous locomotor activity was assessed by infrared beam interruptions within the chamber. Animals were first habituated to the CLAMS chambers for 24 hr with animal housing, lighting, temperature, and diet conditions maintained. For ABHD6$^{NAc\ GFP}$ and ABHD6$^{NAc\ KO}$ animals, body composition and metabolic phenotyping occurred at 8 weeks on diet (10 weeks following surgery), with body weight and food intake assessed every other day. For ABHD6$^{VTA\ GFP}$ and ABHD6$^{VTA\ KO}$ animals, metabolic phenotyping on standard chow diet occurred at 6 weeks following surgery, and metabolic phenotyping and body composition were assessed at 13 weeks following the transition to a high-fat diet (19 weeks following surgery), with body weight and food intake assessed weekly. For ICV WWL70 experiment animals, mice were fed a chow diet and then switched and maintained on HFD following surgery, with body weight and food intake measured 2–3 times/week for 4 weeks. During the 4 weeks with the mini pump, mice were tested for anxiety using the open field test and assessed in echo MRI whole-body composition analyzer and CLAMS to assess energy expenditure. Feed efficiency was calculated as the ratio of the change in body weight (g) divided by cumulative food intake (kcal). For all experiments, measurements for food intake, body weight, and behaviour were taken during the dark cycle.

Home-cage voluntary wheel-running

Mice were individually housed in rat cages to accommodate low-profile, wireless running wheels (ENV-044, Med Associates Inc), with rotation data exported from Wheel Manager Data Acquisition software (Med Associates Inc). For ABHD6$^{NAc\ GFP}$ and ABHD6$^{NAc\ KO}$ on a chow diet, the wheel was introduced 2 weeks following surgery. For ABHD6$^{NAc\ GFP}$ and ABHD6$^{NAc\ KO}$ mice on high-fat diet, wheels were introduced following 8 weeks of HFD feeding (10 weeks following surgery), with HFD feeding continuing during run-wheel access. Run-wheel data was collected for all mice for a period of 26 days.

Elevated plus maze test

The elevated plus maze test was used as a measure of anxiety-like behaviour[175,176]. Mice were placed within the centre of an elevated plus maze apparatus and allowed to freely explore for 5 min. The apparatus included two open arms and two closed arms. Behaviour was video recorded and analyzed using EthoVision software (Noldus), to calculate the percentage of time and entries to the open arm areas of the elevated plus maze apparatus, and velocity.

Open field test

The open field test was used as a measure of anxiety-like behaviour[175,176]. Mice were placed within the centre of an open field arena and allowed to freely explore for 5 min. The open field arena consisted of a square box with opaque walls. Behaviour was video recorded and analyzed using EthoVision software (Noldus), to calculate percentage of time and entries to the centre area of the open field arena, and velocity.

Forced swim test

The FST was used to assess behavioural despair[175,176]. Mice were placed into a clear transparent beaker of water for 6 min. Video recording of behaviour was acquired and analyzed with EthoVision software (Noldus). The first 2 min were used as habituation, with time immobile only assessed during the last 4 min.

Social interaction test

Mice were placed into a 3-chambered apparatus with the side chambers containing an overturned wire mesh cup that was empty

https://doi.org/10.1038/s41467-024-54819-5

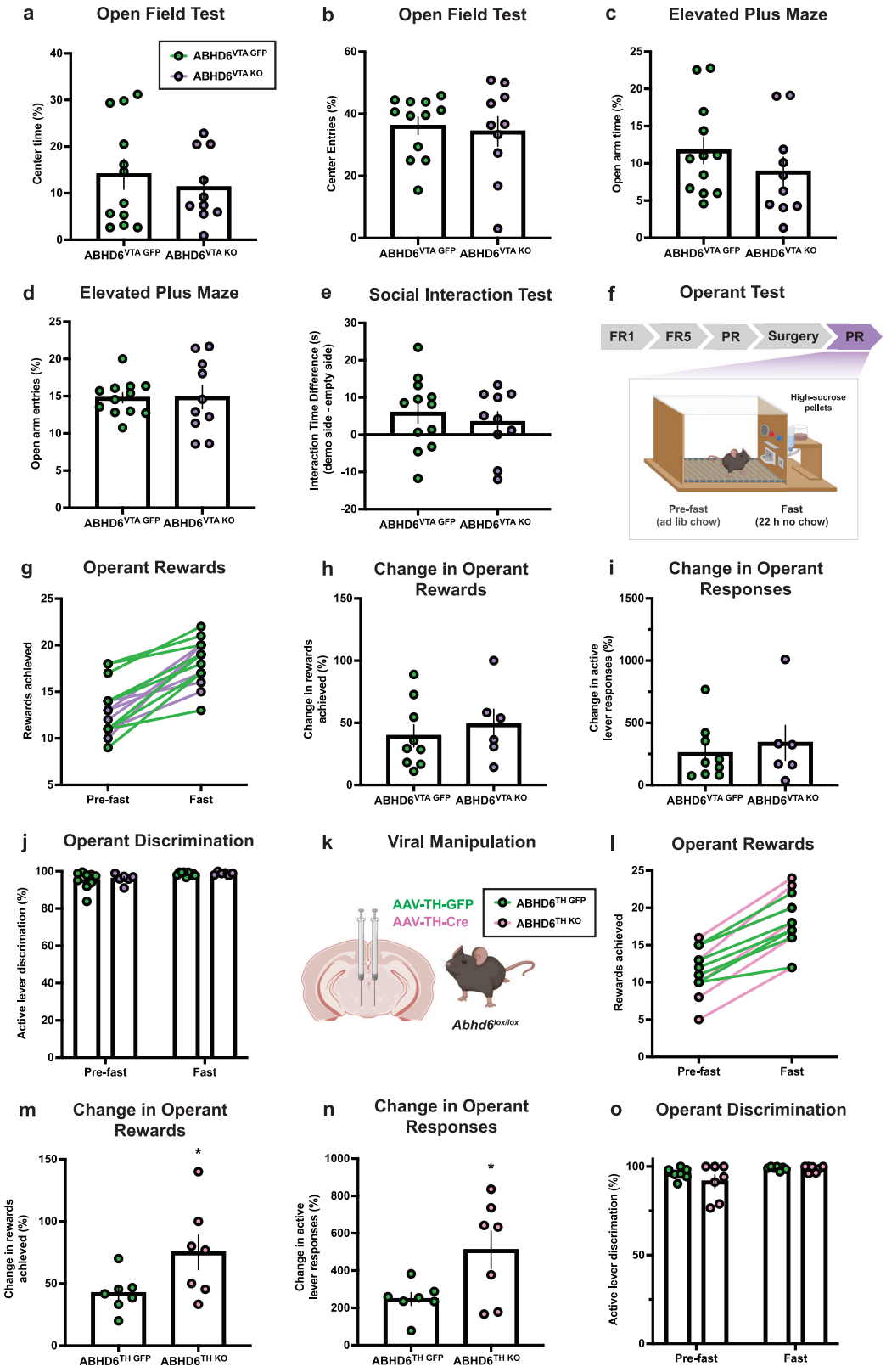

on one side and containing a novel adult male demonstrator mouse (approximately weight matched and of a different genotype) on opposite side. The test mouse was then placed in the centre of the 3-chambered apparatus and allowed to freely explore for 5 min. The demonstrator mouse was changed following every 4 trials, with tests counterbalanced for left/right position of demonstrator mouse. Motor behaviour was video recorded and analyzed using EthoVision software (Noldus). Quantification of the social interaction time was performed manually by visual inspection by a trained individual blinded to both experimental condition and location of the demonstrator mouse. The average of left and right cup interaction times from three independent scoring sessions was used to calculate the interaction time used in statistical analyses.

Fig. 6 | Dopamine neuron ABHD6 deletion enhances food-motivated behaviour. a Proportion of time in centre of the open field ($ABHD6^{VTA\ GFP}$: n = 12, $ABHD6^{VTA\ KO}$: n = 10, P = 0.5143). **b** Proportion of entries into centre of open field ($ABHD6^{VTA\ GFP}$: n = 12, $ABHD6^{VTA\ KO}$: n = 10, P = 0.7379). **c** Proportion of time in open arms of elevated-plus maze ($ABHD6^{VTA\ GFP}$: n = 12, $ABHD6^{VTA\ KO}$: n = 10, P = 0.2961). **d** Proportion of entries into the open arm of the elevated-plus maze ($ABHD6^{VTA\ GFP}$: n = 12, $ABHD6^{VTA\ KO}$: n = 10, P = 0.9518). **e** Difference in interaction time (demonstrator mouse - empty object) in the 3-compartment social interaction task ($ABHD6^{VTA\ GFP}$: n = 12, $ABHD6^{VTA\ KO}$: n = 10, P = 0.5397). **f** Schematic of operant apparatus. FR, fixed ratio; PR, progressive ratio (reinforcement schedule). Created in BioRender. Lau, D. (2023) BioRender.com/t32u518. **g** Operant rewards achieved during operant test prior to and following 22 h fast period ($ABHD6^{VTA\ GFP}$: n = 9, $ABHD6^{VTA\ KO}$: n = 6). **h** Percentage increase in rewards achieved following fast ($ABHD6^{VTA\ GFP}$: n = 9, $ABHD6^{VTA\ KO}$: n = 6, P = 0.5354). **i** Percentage increase in operant lever responses following fast ($ABHD6^{VTA\ GFP}$: n = 9, $ABHD6^{VTA\ KO}$: n = 6, P = 0.5883). **j** Active lever discrimination pre-fast ($ABHD6^{VTA\ GFP}$: n = 9, $ABHD6^{VTA\ KO}$: n = 6, P = 0.7286) and post-fast ($ABHD6^{VTA\ GFP}$: n = 9, $ABHD6^{VTA\ KO}$: n = 6, P = 0.6898). **k** Schematic of viral manipulation for DA neuron-specific ABHD6 loss-of function in VTA. Created in BioRender. Lau, D. (2023) BioRender.com/b72p693. **l** Operant rewards achieved during operant test prior to and following 22 h fast period ($ABHD6^{TH\ GFP}$: n = 7, $ABHD6^{TH\ KO}$: n = 7). **m**. Percentage increase in rewards achieved following fast ($ABHD6^{TH\ GFP}$: n = 7, $ABHD6^{TH\ KO}$: n = 7, P = 0.0494). **n** Percentage increase in operant active lever responses following fast ($ABHD6^{TH\ GFP}$: n = 7, $ABHD6^{TH\ KO}$: n = 7, P = 0.0310). **o** Active lever discrimination pre-fast ($ABHD6^{TH\ GFP}$: n = 7, $ABHD6^{TH\ KO}$: n = 7, P = 0.2831) and post-fast ($ABHD6^{TH\ GFP}$: n = 7, $ABHD6^{TH\ KO}$: n = 7, P = 0.7294). Data represented as mean, with error bars ± SEM; *p < 0.05. Unpaired two-sided t-test (**a–e, h–j, m–o**). Additional details on statistical tests are available in Supplementary Information. Source data are provided as a Source Data file.

Operant testing

All operant training and tests were conducted in the dark cycle in mouse operant boxes (Med Associates Inc), with left/right active lever position counterbalanced across mice[172]. High-sugar pellets (Bio-Serv) were used as food rewards during operant behaviour[172]. Animals were food-restricted on a standard chow diet to approximately 90% of free-feeding body weight during the initial part of operant training up to the acquisition of fixed-ratio (FR) 1 schedule reinforcement, then returned to an ad libitum chow feeding schedule throughout later stages of training and testing[172]. For NAc experimental mice, training proceeded from FR1, to FR3, then FR5 schedules of reinforcement. Following training mice received intra-NAc AAV injections to generate $ABHD6^{NAc\ GFP}$ and $ABHD6^{NAc\ KO}$ mice. Following two weeks of recovery from surgery mice received 1-2 sessions of operant behaviour at FR1, followed by remaining sessions at FR5. The mean of the first three stable days of responding was assessed for each group. For VTA experimental mice, training proceeded from FR1, FR5, then progressive ratio (PR), using formula from[172]. Following stable responding, mice received intra-VTA injections to generate either $ABHD6^{VTA\ GFP}$ and $ABHD6^{VTA\ KO}$ mice or $ABHD6^{TH\ GFP}$ and $ABHD6^{TH\ KO}$ mice. Following two weeks of recovery from surgery mice were returned to PR operant sessions until mice achieved stable responding. The magnitude of changes in rewards achieved and active lever operant responses were additionally assessed between a fasted state (following the 22 hr fast) and the sated state from the previous day, in which animals had ad libitum access to home-cage chow prior to testing.

Amphetamine conditioned place preference

Prior to conditioning, mice received 1–2 preconditioning sessions during which they were confined to each of the conditioning sides in a 3-compartment fully automated chamber (Med Associates Inc) for 15 min. Following preconditioning animals were placed in the centre of the apparatus and allowed to freely explore (pre-conditioning preference). Animals demonstrating a preference above 40% for one compartment were not used. Saline- and amphetamine-conditioning chambers in the apparatus were assigned in a counterbalanced manner. For conditioning mice received two 15-minute conditioning periods confined to each of the lateral chambers, repeated for 4 days. Each daily conditioning session included a saline-paired session, followed by an amphetamine-paired session in the opposite lateral chamber at 2 h following saline session. Injection of saline or amphetamine (2 mg/kg, i.p., Sigma-Aldrich) occurred 5 min prior to placement in the conditioning chamber. Conditioned place preference was assessed on the following day at 22 hr – 24 hr, at the midpoint (~23 hr) between the two daily conditioning sessions the preceding day, with mice allowed to freely explore the apparatus for 15 min. Preference was calculated as the percentage time spent in amphetamine-conditioned compartment of the 3-box chamber.

Electrophysiology

Coronal slices (250 µm) containing the NAc were obtained using a vibratome (Leica VT1200S) in a solution containing: 210 mM sucrose, 7 mM D-glucose, 25 mM $NaHCO_3$, 1.25 mM NaH_2PO_4, 2.5 mM KCl, 1.3 mM Na-ascorbate, 3 mM Na-pyruvate, 0.5 mM $CaCl_2$, 7 mM $MgCl_2$, saturated with 95% O_2/5% CO_2. Slices were allowed to recover at 30 °C for 30 min, and subsequently at room temperature, in a solution containing: 118 mM NaCl, 11 mM D-glucose, 26 mM $NaHCO_3$, 15 mM HEPES, 1.25 mM NaH_2PO_4, 2.5 mM KCl, 0.4 mM Na-ascorbate, 3 mM myo-inositol, 2 mM Na-pyruvate, 2 mM $CaCl_2$, 1 mM $MgCl_2$, saturated with 95% O_2/5% CO_2. Whole-cell patch-clamp recordings were obtained from $ABHD6^{NAc\ GFP}$ and $ABHD6^{NAc\ KO}$ mice between 1.5 h and 6 h after slicing. Perfusate (~1.5 ml/min at 30 ± 1 °C) contained: 119 mM NaCl, 26.2 mM $NaHCO_3$, 11 mM glucose, 2.5 mM KCl, 1 mM NaH_2PO_4, 2.5 mM $CaCl_2$, and 1.3 mM $MgCl_2$, saturated with 95% O_2/5% CO_2. Cells were patched using borosilicate glass pipettes (2–4 MΩ) filled with: 127 mM CsCl, 8 mM NaCl, 1 mM $CaCl_2$, 10 mM EGTA, 10 mM HEPES, 0.3 mM Na_3-GTP, and 2 mM Mg-ATP, pH 7.2 for inhibitory post synaptic currents (IPSCs) or 135 mM $CsMeSO_4$, 8 mM NaCl, 0.6 mM EGTA, 10 mM HEPES, 0.3 mM Na_3-GTP, 4 mM Mg-ATP, and 5 mM QX-314, pH 7.3 for excitatory postsynaptic synaptic currents (EPSCs). IPSPs and EPSPs were amplified and filtered (2 kHz) using an Axopatch 200B amplifier, sampled at 10 kHz using a Digidata 1440 A, and recorded with Clampex 10.3 (Molecular Devices). To isolate mIPSCs, 0.5 µm TTX, 10 µm NBQX, and 25 µm d-APV were added to the perfusate, whereas TTX was omitted for s/eIPSCs. To isolate s/eEPSCs, 50 µM PTX was added to the perfusate. Recordings were performed at V_h = −70 mV. Evoked responses were generated using borosilicate glass pipette stimulators (~20–30 µm open tip diameter) filled with external solution and positioned 100-300 µm away from the recorded cell. Analyses were performed using Clampfit 10.3 (Molecular Devices). Passive membrane properties and access resistance were assessed between each sweep. Only cells with a stable access resistance (<20% change, <25 MΩ) throughout the recording period were included in the analysis. Average access resistance did not differ significantly across groups (p > 0.60).

Tissue collection and quantitative real-time PCR

RT-qPCR experiments were performed to assess RNA content within the NAc and VTA[175]. Mice were sacrificed during the dark phase under isoflurane anaesthesia with rapid brain extraction. Brains were rapidly frozen and stored at −80 °C until cryosectioning. Tissue punches containing the NAc and/or the VTA were acquired using a biopsy punch from serial frozen coronal sections (100-200 µm) and stored at −80 °C. Tissue was homogenized and RNA extracted using TRIzol (Invitrogen), and cDNA prepared using random hexamers (GeneLink) and M-MLV Reverse Transcriptase (Invitrogen). Real-time quantitative-

https://doi.org/10.1038/s41467-024-54819-5

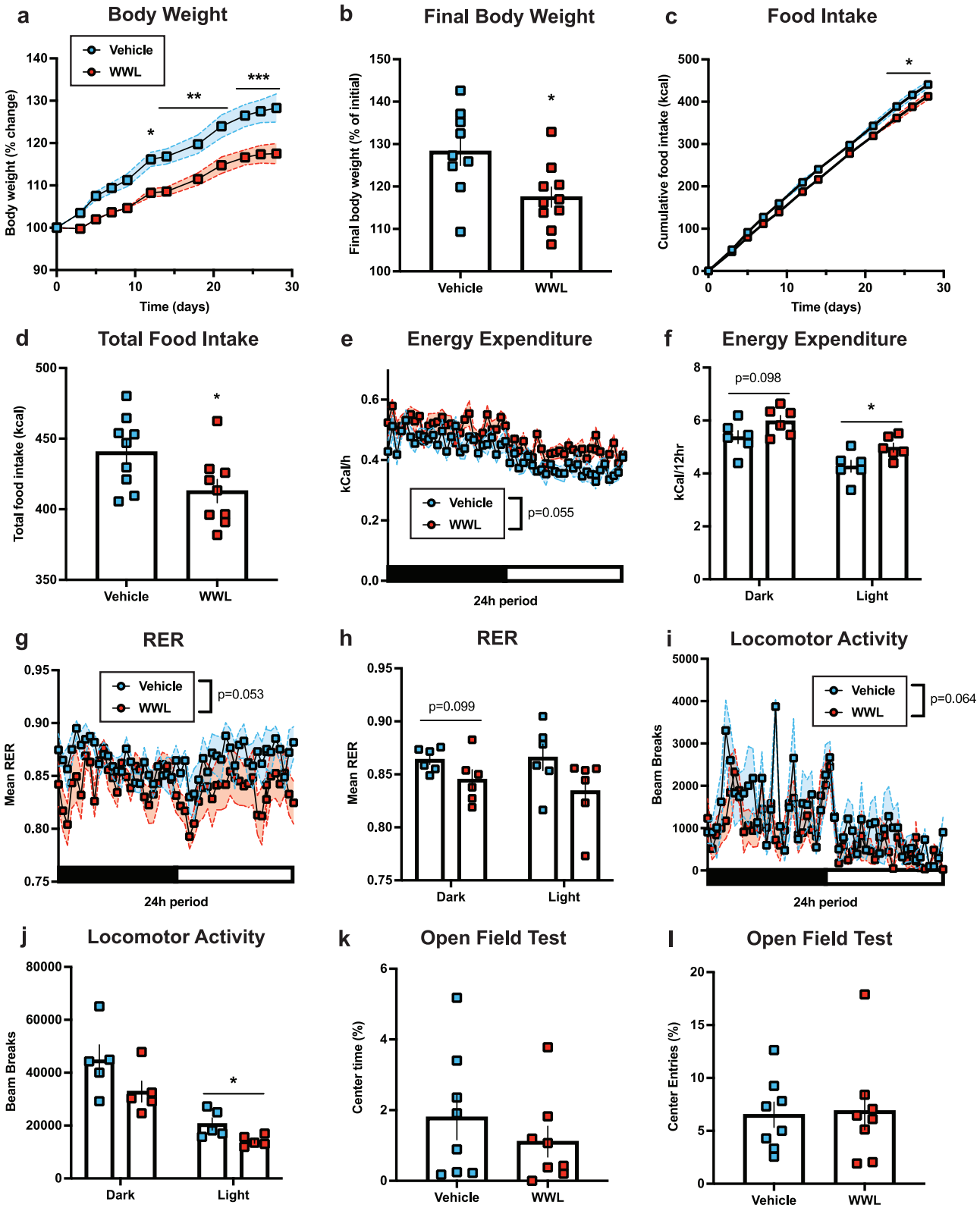

PCR reactions were performed with Rotor Gene SYBR Green PCR (Qiagen) and SsoAdvanced Universal SYBR Green Supermix (Bio-Rad). Primers used for RT-qPCR experiments are listed in the Supplementary Information (Supplementary Table 2). For all NAc experiments, expression was normalized to 18 s. For VTA gene expression experiments, the most stable reference gene combination was selected using NormFinder software[177]. All RT-qPCR data is expressed as relative fold change to control group normalized at 1.0.

Liquid chromatography/mass spectrometry

High-performance liquid chromatography with tandem mass spectrometry/mass spectrometry (HPLC tandem MS/MS) was performed for quantitative analysis of NAc endocannabinoid levels[53]. Two weeks following injection of either AAV-hSyn-Cre or AAV-hSyn-GFP, NAc sections were rapidly extracted and snap frozen in liquid nitrogen and stored at −80 °C. Precellys 3D-homogenizer (Bertin Technologies) was used to homogenize tissue at 5500 rpm for 25 s at 4 °C in buffer

Fig. 7 | Central pharmacological inhibition of ABHD6 suppresses body weight gain on a high-fat diet via reduced food intake and enhanced energy expenditure. a Body weight on HFD (VEH: n = 9, WWL: n = 10, two-way ANOVA interaction P < 0.0001). **b** Final body weight (VEH: n = 9, WWL: n = 10, P = 0.0160). **c** Food intake (VEH: n = 9, WWL: n = 9, two-way ANOVA interaction P = 0.0001). **d** Total food intake (VEH: n = 9, WWL: n = 9, P = 0.0332). **e** Energy expenditure (VEH: n = 6, WWL: n = 6, two-way ANOVA group main effect P = 0.0552). **f** Energy expenditure in (**e**) during dark (VEH: n = 6, WWL: n = 6, P = 0.0978) or light cycle (VEH: n = 6, WWL: n = 6, P = 0.0307). **g** Respiratory exchange ratio (VEH: n = 6, WWL: n = 6, two-way ANOVA group main effect P = 0.0533). **h** Mean RER in (**g**) during dark (VEH: n = 6, WWL: n = 6, P = 0.0986) or light cycle (VEH: n = 6, WWL: n = 6, P = 0.1118). **i** Locomotor activity (VEH: n = 5, WWL: n = 5, two-way ANOVA group main effect P = 0.0636). **j** Locomotor activity in (i) during dark (VEH: n = 5, WWL: n = 5, P = 0.1313) or light cycle (VEH: n = 5, WWL: n = 5, P = 0.0326). **k** Percentage time in centre area (VEH: n = 8, WWL: n = 8, P = 0.3868). **l** Percentage entries to centre area (VEH: n = 8, WWL: n = 8, P = 0.8711). Data represented as mean, with error bars/shaded areas ± SEM; *p < 0.05, **p < 0.01, ***p < 0.001. Unpaired two-sided t-test (**b**, **d**, **f**, **h**, **j**–**l**), two-way ANOVA group x time interaction with Sidak's post hoc correction (**a**, **c**), two-way ANOVA group main effect (**e**, **g**, **i**). Additional details on statistical tests are available in Supplementary Information. Source data are provided as a Source Data file.

(200 mM sucrose, 50 mM Tris-HCL, 5 mM $MgCl_2$, 2.5 mM EDTA, pH 7.4) containing 66% v/v toluene spiked with 10 ng deuterium labelled 2-AG internal standard (2-AG-d5). At 4 °C two successive liquid-liquid extractions were performed with 2 and 1 volumes of toluene. Centrifugation at 3500 *g* for 15 min at 4 °C was performed for phase separation, after which the upper two phases were prepared in a salinized glass tube and dried under nitrogen. Dried organic extracts were reconstituted in 40 µl of 2 mM ammonium acetate in methanol and 2 mM ammonium acetate in water (4:1, v/v). Samples were vortexed for 15 s and centrifuged for 5 min at 13000 *g*, and 30 µl of clear supernatant was transferred to a salinized insert in a vial for quantitative analysis performed on Agilent 1200 SL system coupled to a triple quadrupole mass spectrometer (4000Q TRAP MS/MS, SCIEX). Samples were resolved on Zorbax Eclipse Plus-C18 column (2.1 mm x 100 mm, 1.8 µm particle size; Agilent Technologies) at 0.35 ml/min at 60 °C column temperature, with the mobile phase including solvent A (2 mM ammonium acetate in water) and solvent B (2 mM ammonium acetate in methanol). The gradient applied was: 0.0 to 0.5 min 80% B, 0.5 to 6.0 min to 87% B, 6.0 to 7.2 min to 100% B, and 7.2 to 9.0 min 80% B. The MS was operated in positive electrospray ionization mode using a turbo ion spray source, and 2-AG/1-AG and 2-AG-d5 were measured on multiple reaction monitoring mode (MRM). Compound optimization of 2-AG/1-AG was based on fragmentation of the precursor ion 379.3 m/z that yielded a prominent product ion at 287.5 m/z. 2-AG-d5 internal standard optimization reported the 384.5 m/z precursor ion that yielded the predominant 287.5 m/z fragment. Quantification was performed by integrating peak areas from selected transitions (Multiquant software, version 2.0.2, SCIEX), with 2-AG levels determined using a specific standard curve. Due to rapid isomerization of 2-AG into 1-AG in biological matrix[178], 2-AG was quantified as the sum of 2-AG and 1-AG.

Immunostaining and image analysis

Two weeks following surgery, mice were perfused under sodium pentobarbital with 10 mL of saline, followed by 10 mL of 10% neutral buffered formalin (NBF). Brains were post-fixed for 3–4 hr at room temperature, and cryoprotected in serial overnight storages of 10%, 20%, and 30% sucrose solutions in 1X PBS at 4 °C, then frozen and stored at −80 °C. Coronal sections at 25–30µm thickness were taken from the NAc or VTA on sliding microtome (Leica SM2000R). Free-floating sections were immunostained rinsed in PBS, permeabilized in 0.2% PBS-Triton, rinsed in PBS, blocked in 3% goat serum for 2 hr at room temperature, and incubated in anti-GFP (1:2000; Invitrogen, A6455) and anti-NeuN (1:500; Millipore, MAB377) primary antibodies overnight at 4 °C. Sections were rinsed and incubated in secondary Alexa Fluor antibodies (1:500, ThermoFisher) for 2 hr at room temperature, rinsed, mounted and coverslipped with hardset medium with DAPI (Vector Laboratories). Sections were imaged using consistent laser power and imaging settings on a fluorescent microscope (Zeiss Axio Imager M2) at 10x primary magnification. For visualization purposes only, brightness and contrast were adjusted in representative photomicrographs used in Fig. 1c with ImageJ.

RNA in situ hybridization and image analysis

For NAc RNAscope experiments, adult male C57BL/6 J mice (Jackson) were perfused under sodium pentobarbital anaesthesia (200 mg/kg, IP) with ice-cold PBS and 10% NBF. Brains were post-fixed overnight at 4 °C and cryoprotected in 10, 20, and 30% successive sucrose solutions in 1x PBS for ~24 hr each, prior to freezing for cryosectioning. Fixed-frozen tissue was sectioned on a microtome (Leica SM2000R) at 30 µm thickness, and stored at −80 °C. RNA in situ hybridization was performed with RNAscope Fluorescent Multiplex Assay (V2) on tissue sections containing the NAc around +1.0 mm bregma, according to manufacturer protocols (UM 323100). *Abhd6* (Channel 1) and *Slc32a1* (Channel 3) were visualized with Opal570 and Opal690, respectively. For VTA RNAscope experiments, adult male *Abhd6*$^{lox/lox}$ mice were sacrificed under isoflourane anaesthesia with brains rapidly removed, frozen and placed within an optimal cutting temperature solution frozen in 2-methylbutane with dry ice and stored at −80 °C until cryosectioning. Fresh-frozen tissue was sectioned on a cryostat (Leica CM3050 S) at 18 µm thickness around −20 °C, and stored on slides at −80 °C. RNA in situ hybridization was performed with RNAscope Fluorescent Multiplex Assay (V1) on tissue sections containing the VTA around −3.4 mm bregma, according to manufacturer protocols (320513-USM, 320293-UM), with the exception that tissue fixation was performed in 10% NBF at room temperature for 30 min. *Abhd6* (Channel 1) and *Th* (Channel 2) were visualized using Amp4 Alt C Fluorescent Labels. For each experiment all slides were imaged using consistent laser power and imaging settings on a fluorescent microscope (Zeiss Axio Imager M2, Zeiss). For NAc RNAscope experiments, z-stack images were acquired, with the maximum intensity projection obtained using ImageJ. For visualization purposes only, brightness and contrast were adjusted in representative photomicrographs used in Fig. 5a with ImageJ.

Exclusion criteria

Outliers were removed based on pre-determined criteria (p < 0.05) with Grubb's test (Outlier calculator; GraphPad, Boston, MA, USA). For VTA pan-neuronal ABHD6 deletion experiments, mice with relative ABHD6 expression above the mean (>1.0) of the control group (ABHD6$^{VTA\ GFP}$) were excluded from analysis. For operant experiments, mice that did not achieve criterion for active lever discrimination above 70% were excluded from analyses.

Statistical analyses

All statistical analyses were conducted using Prism 9 (GraphPad Software, Boston, MA, USA). Graphed data are represented as mean ± SEM, unless indicated otherwise. Data analysis on body weight, cumulative food intake, locomotor activity, energy expenditure, and RER as a function of time, and m/eIPSC as a function of time were analyzed with two-way repeated measures mixed analysis of variance (ANOVA), with between-subjects factor of viral condition or pharmacological treatment and within-subjects factor of time. Multiple comparisons with Sidak's test were used for post-hoc analyses when justified. Running-wheel data were analyzed with one-way ANOVA with between-subjects factor of viral/diet condition and within-subjects factor of time, with

multiple comparisons with Tukey's test for post-hoc analyses when justified. All other data was analyzed using unpaired two-tailed t-test. Differences were considered significant at $p < 0.05$. Asterisks indicate $^{*}p < 0.05$, $^{**}p < 0.01$, $^{***}p < 0.001$, and $^{****}p < 0.0001$. Results of statistical tests are listed in the Supplementary Information (Supplementary Tables 3–14).

Data availability

All data supporting the findings of the study are available within the main text, the Supplementary Information and the Source Data files that accompany this article.

References

1. Piazza, P. V., Cota, D. & Marsicano, G. The CB1 receptor as the Cornerstone of Exostasis. *Neuron* **93**, 1252–1274 (2017).
2. Loos, R. J. F. & Yeo, G. S. H. The genetics of obesity: from discovery to biology. *Nat. Rev. Genet* **23**, 120–133 (2022).
3. Poursharifi, P., Madiraju, S. R. M. & Prentki, M. Monoacylglycerol signalling and ABHD6 in health and disease. *Diab., Obes. Metab.* **19**, 76–89 (2017).
4. Blankman, J. L., Simon, G. M. & Cravatt, B. F. A comprehensive profile of brain enzymes that hydrolyze the Endocannabinoid 2-Arachidonoylglycerol. *Chem. Biol.* **14**, 1347–1356 (2007).
5. Marrs, W. R. et al. The serine hydrolase ABHD6 controls the accumulation and efficacy of 2-AG at cannabinoid receptors. *Nat. Neurosci.* **13**, 951–957 (2010).
6. Cao, J. K., Kaplan, J. & Stella, N. ABHD6: Its place in Endocannabinoid signaling and beyond. *Trends Pharm. Sci.* **40**, 267–277 (2019).
7. Fulton, S. Appetite and reward. *Front Neuroendocrinol.* **31**, 85–103 (2010).
8. Volkow, N. D., Wise, R. A. & Baler, R. The dopamine motive system: implications for drug and food addiction. *Nat. Rev. Neurosci.* **18**, 741–752 (2017).
9. Parsons, L. H. & Hurd, Y. L. Endocannabinoid signalling in reward and addiction. *Nat. Rev. Neurosci.* **16**, 579–594 (2015).
10. Lau, B. K., Cota, D., Cristino, L. & Borgland, S. L. Endocannabinoid modulation of homeostatic and non-homeostatic feeding circuits. *Neuropharmacology* **124**, 38–51 (2017).
11. Peters, K. Z., Oleson, E. B. & Cheer, J. F. A Brain on Cannabinoids: The role of dopamine release in reward seeking and addiction. *Cold Spring Harb. Perspect. Med.* **11**, https://doi.org/10.1101/cshperspect.a039305 (2021).
12. Covey, D. P. & Yocky, A. G. Endocannabinoid modulation of nucleus accumbens microcircuitry and terminal Dopamine release. *Front Synaptic Neurosci.* **13**, 734975 (2021).
13. Mátyás, F. et al. Identification of the sites of 2-arachidonoylglycerol synthesis and action imply retrograde endocannabinoid signaling at both GABAergic and glutamatergic synapses in the ventral tegmental area. *Neuropharmacology* **54**, 95–107 (2008).
14. Burgdorf, C. E. et al. Endocannabinoid genetic variation enhances vulnerability to THC reward in adolescent female mice. *Sci. Adv.* **6**, eaay1502 (2020).
15. Melis, M. et al. Endocannabinoids mediate presynaptic inhibition of glutamatergic transmission in rat ventral tegmental area dopamine neurons through activation of CB1 receptors. *J. Neurosci.* **24**, 53–62 (2004).
16. Cheer, J. F., Wassum, K. M., Heien, M. L., Phillips, P. E. & Wightman, R. M. Cannabinoids enhance subsecond dopamine release in the nucleus accumbens of awake rats. *J. Neurosci.* **24**, 4393–4400 (2004).
17. Bossong, M. G. et al. Further human evidence for striatal dopamine release induced by administration of Δ9-tetrahydrocannabinol (THC): selectivity to limbic striatum. *Psychopharmacology* **232**, 2723–2729 (2015).
18. Tung, L.-W. et al. Orexins contribute to restraint stress-induced cocaine relapse by endocannabinoid-mediated disinhibition of dopaminergic neurons. *Nat. Commun.* **7**, 12199 (2016).
19. Luján, M. Á. et al. Mobilization of endocannabinoids by midbrain dopamine neurons is required for the encoding of reward prediction. *Nat. Commun.* **14**, 7545 (2023).
20. Oleson, E. B. et al. Endocannabinoids shape accumbal encoding of cue-motivated behavior via CB1 receptor activation in the ventral tegmentum. *Neuron* **73**, 360–373 (2012).
21. Oleson, E. B. et al. Cannabinoid receptor activation shifts temporally engendered patterns of dopamine release. *Neuropsychopharmacology* **39**, 1441–1452 (2014).
22. Wang, H., Treadway, T., Covey, D. P., Cheer, J. F. & Lupica, C. R. Cocaine-induced endocannabinoid mobilization in the ventral tegmental area. *Cell Rep.* **12**, 1997–2008 (2015).
23. Wenzel, J. M. et al. Phasic Dopamine signals in the nucleus accumbens that cause active avoidance require Endocannabinoid mobilization in the midbrain. *Curr. Biol.* **28**, 1392–1404.e1395 (2018).
24. Bacharach, S. Z. et al. Decreased ventral tegmental area CB1R signaling reduces sign tracking and shifts cue-outcome dynamics in rat nucleus Accumbens. *J. Neurosci.* **43**, 4684–4696 (2023).
25. Ward, S. J., Walker, E. A. & Dykstra, L. A. Effect of Cannabinoid CB1 receptor antagonist SR141714A and CB1 receptor knockout on cue-induced reinstatement of Ensure® and corn-oil seeking in mice. *Neuropsychopharmacology* **32**, 2592–2600 (2007).
26. Hernandez, G. & Cheer, J. F. Effect of CB1 receptor blockade on food-reinforced responding and associated nucleus accumbens neuronal activity in rats. *J. Neurosci.* **32**, 11467–11477 (2012).
27. Covey, D. P. et al. Inhibition of endocannabinoid degradation rectifies motivational and dopaminergic deficits in the Q175 mouse model of Huntington's disease. *Neuropsychopharmacology* **43**, 2056–2063 (2018).
28. Feja, M. et al. The novel MAGL inhibitor MJN110 enhances responding to reward-predictive incentive cues by activation of CB1 receptors. *Neuropharmacology* **162**, 107814 (2020).
29. Covey, D. P., Hernandez, E., Luján, M. Á. & Cheer, J. F. Chronic augmentation of Endocannabinoid levels persistently increases dopaminergic encoding of reward cost and motivation. *J. Neurosci.* **41**, 6946 (2021).
30. Gerfen, C. R. & Surmeier, D. J. Modulation of striatal projection systems by dopamine. *Annu Rev. Neurosci.* **34**, 441–466 (2011).
31. Robbe, D., Kopf, M., Remaury, A., Bockaert, J. & Manzoni, O. J. Endogenous cannabinoids mediate long-term synaptic depression in the nucleus accumbens. *Proc. Natl Acad. Sci.* **99**, 8384–8388 (2002).
32. Uchigashima, M. et al. Subcellular arrangement of molecules for 2-Arachidonoyl-Glycerol-mediated retrograde signaling and its physiological contribution to synaptic modulation in the Striatum. *J. Neurosci.* **27**, 3663 (2007).
33. Tanimura, A. et al. The endocannabinoid 2-arachidonoylglycerol produced by diacylglycerol lipase alpha mediates retrograde suppression of synaptic transmission. *Neuron* **65**, 320–327 (2010).
34. Shen, C. J. et al. Cannabinoid CB(1) receptors in the amygdalar cholecystokinin glutamatergic afferents to nucleus accumbens modulate depressive-like behavior. *Nat. Med.* **25**, 337–349 (2019).
35. Deroche, M. A., Lassalle, O., Castell, L., Valjent, E. & Manzoni, O. J. Cell-Type- and Endocannabinoid-specific synapse connectivity in the adult nucleus accumbens core. *J. Neurosci.* **40**, 1028 (2020).
36. Hwang, E. K. & Lupica, C. R. Altered Corticolimbic control of the nucleus accumbens by long-term Δ(9)-Tetrahydrocannabinol exposure. *Biol. Psychiatry* **87**, 619–631 (2020).

37. Folkes, O. M. et al. An endocannabinoid-regulated basolateral amygdala-nucleus accumbens circuit modulates sociability. *J. Clin. Invest* **130**, 1728–1742 (2020).
38. Narushima, M., Uchigashima, M., Hashimoto, K., Watanabe, M. & Kano, M. Depolarization-induced suppression of inhibition mediated by endocannabinoids at synapses from fast-spiking interneurons to medium spiny neurons in the striatum. *Eur. J. Neurosci.* **24**, 2246–2252 (2006).
39. Winters, B. D. et al. Cannabinoid receptor 1-expressing neurons in the nucleus accumbens. *Proc. Natl Acad. Sci.* **109**, E2717–E2725 (2012).
40. Mathur, B. N., Tanahira, C., Tamamaki, N. & Lovinger, D. M. Voltage drives diverse endocannabinoid signals to mediate striatal microcircuit-specific plasticity. *Nat. Neurosci.* **16**, 1275–1283 (2013).
41. Wright, W. J., Schlüter, O. M. & Dong, Y. A feedforward inhibitory circuit mediated by CB1-Expressing fast-spiking interneurons in the nucleus accumbens. *Neuropsychopharmacology* **42**, 1146–1156 (2017).
42. Yu, J. et al. Nucleus accumbens feedforward inhibition circuit promotes cocaine self-administration. *Proc. Natl Acad. Sci. USA* **114**, E8750–e8759 (2017).
43. Freiman, I., Anton, A., Monyer, H., Urbanski, M. J. & Szabo, B. Analysis of the effects of cannabinoids on identified synaptic connections in the caudate-putamen by paired recordings in transgenic mice. *J. Physiol.* **575**, 789–806 (2006).
44. Buczynski, M. W. et al. Diacylglycerol lipase disinhibits VTA dopamine neurons during chronic nicotine exposure. *Proc. Natl Acad. Sci.* **113**, 1086–1091 (2016).
45. Davis, M. I. et al. The cannabinoid-1 receptor is abundantly expressed in striatal striosomes and striosome-dendron bouquets of the substantia nigra. *PLoS One* **13**, e0191436 (2018).
46. Fulton, S., Décarie-Spain, L., Fioramonti, X., Guiard, B. & Nakajima, S. The menace of obesity to depression and anxiety prevalence. *Trends Endocrinol. Metab.* **33**, 18–35 (2022).
47. Bara, A., Ferland, J. N., Rompala, G., Szutorisz, H. & Hurd, Y. L. Cannabis and synaptic reprogramming of the developing brain. *Nat. Rev. Neurosci.* **22**, 423–438 (2021).
48. Frau, R. et al. Prenatal THC exposure produces a hyperdopaminergic phenotype rescued by pregnenolone. *Nat. Neurosci.* **22**, 1975–1985 (2019).
49. Metna-Laurent, M., Mondésir, M., Grel, A., Vallée, M. & Piazza, P. V. Cannabinoid-Induced Tetrad in Mice. *Curr. Protoc. Neurosci.* **80**, 9.59.51–59.59.10 (2017).
50. Busquets-García, A., Bolaños, J. P. & Marsicano, G. Metabolic Messengers: endocannabinoids. *Nat. Metab.* **4**, 848–855 (2022).
51. Saunders, A. et al. Molecular diversity and specializations among the cells of the adult mouse brain. *Cell* **174**, 1015–1030.e1016 (2018).
52. Savell, K. E. et al. A dopamine-induced gene expression signature regulates neuronal function and cocaine response. *Sci. Adv.* **6**, eaba4221 (2020).
53. Fisette, A. et al. α/β-Hydrolase Domain 6 in the Ventromedial Hypothalamus controls energy metabolism flexibility. *Cell Rep.* **17**, 1217–1226 (2016).
54. Zhao, S. et al. α/β-Hydrolase domain-6-accessible monoacylglycerol controls glucose-stimulated insulin secretion. *Cell Metab.* **19**, 993–1007 (2014).
55. Phillips, R. A. et al. An atlas of transcriptionally defined cell populations in the rat ventral tegmental area. *Cell Rep.* **39**, 110616 (2022).
56. Schlosburg, J. E. et al. Chronic monoacylglycerol lipase blockade causes functional antagonism of the endocannabinoid system. *Nat. Neurosci.* **13**, 1113–1119 (2010).
57. Fuss, J. et al. A runner's high depends on cannabinoid receptors in mice. *Proc. Natl Acad. Sci. USA* **112**, 13105–13108 (2015).
58. Dubreucq, S. et al. Ventral tegmental area cannabinoid type-1 receptors control voluntary exercise performance. *Biol. Psychiatry* **73**, 895–903 (2013).
59. Muguruza, C. et al. The motivation for exercise over palatable food is dictated by cannabinoid type-1 receptors. *JCI Insight* **4**, https://doi.org/10.1172/jci.insight.126190 (2019).
60. Siebers, M., Biedermann, S. V., Bindila, L., Lutz, B. & Fuss, J. Exercise-induced euphoria and anxiolysis do not depend on endogenous opioids in humans. *Psychoneuroendocrinology* **126**, 105173 (2021).
61. Oleson, E. B., Hamilton, L. R. & Gomez, D. M. Cannabinoid modulation of Dopamine release during motivation, periodic reinforcement, exploratory behavior, habit formation, and attention. *Front Synaptic Neurosci.* **13**, 660218 (2021).
62. Wang, W. et al. Deficiency in endocannabinoid signaling in the nucleus accumbens induced by chronic unpredictable stress. *Neuropsychopharmacology* **35**, 2249–2261 (2010).
63. Lafourcade, M. et al. Nutritional omega-3 deficiency abolishes endocannabinoid-mediated neuronal functions. *Nat. Neurosci.* **14**, 345–350 (2011).
64. Bosch-Bouju, C., Larrieu, T., Linders, L., Manzoni, O. J. & Layé, S. Endocannabinoid-mediated plasticity in nucleus accumbens controls vulnerability to anxiety after social defeat stress. *Cell Rep.* **16**, 1237–1242 (2016).
65. Dudek, K., et al. Astrocytic cannabinoid receptor 1 promotes resilience by dampening stress-induced blood-brain barrier alterations. *Res. Square*, https://doi.org/10.21203/rs.3.rs-2978353/v1 (2023).
66. Friend, D. M. et al. Basal Ganglia dysfunction contributes to physical inactivity in obesity. *Cell Metab.* **25**, 312–321 (2017).
67. Kim, J. & Alger, B. E. Reduction in endocannabinoid tone is a homeostatic mechanism for specific inhibitory synapses. *Nat. Neurosci.* **13**, 592–600 (2010).
68. Pribiag, H. & Stellwagen, D. Neuroimmune regulation of homeostatic synaptic plasticity. *Neuropharmacology* **78**, 13–22 (2014).
69. Morena, M., Patel, S., Bains, J. S. & Hill, M. N. Neurobiological interactions between stress and the Endocannabinoid system. *Neuropsychopharmacology* **41**, 80–102 (2016).
70. Zhao, S. et al. α/β-Hydrolase Domain 6 deletion induces adipose browning and prevents obesity and Type 2 Diabetes. *Cell Rep.* **14**, 2872–2888 (2016).
71. Zhong, P. et al. Monoacylglycerol lipase inhibition blocks chronic stress-induced depressive-like behaviors via activation of mTOR signaling. *Neuropsychopharmacology* **39**, 1763–1776 (2014).
72. Manduca, A. et al. Amplification of mGlu(5)-Endocannabinoid signaling rescues behavioral and synaptic deficits in a mouse model of adolescent and adult dietary polyunsaturated fatty acid imbalance. *J. Neurosci.* **37**, 6851–6868 (2017).
73. Hsu, T. M., McCutcheon, J. E. & Roitman, M. F. Parallels and overlap: the integration of homeostatic signals by mesolimbic dopamine neurons. *Front Psychiatry* **9**, 410 (2018).
74. Fulton, S. et al. Leptin regulation of the mesoaccumbens dopamine pathway. *Neuron* **51**, 811–822 (2006).
75. Morales, M. & Margolis, E. B. Ventral tegmental area: cellular heterogeneity, connectivity and behaviour. *Nat. Rev. Neurosci.* **18**, 73–85 (2017).
76. Tan, K. R. et al. GABA neurons of the VTA drive conditioned place aversion. *Neuron* **73**, 1173–1183 (2012).
77. van Zessen, R., Phillips, J. L., Budygin, E. A. & Stuber, G. D. Activation of VTA GABA neurons disrupts reward consumption. *Neuron* **73**, 1184–1194 (2012).
78. Friend, L. et al. CB1-dependent long-term depression in ventral tegmental area GABA Neurons: A novel target for Marijuana. *J. Neurosci.* **37**, 10943–10954 (2017).
79. Li, W., Blankman, J. L. & Cravatt, B. F. A functional proteomic strategy to discover inhibitors for uncharacterized hydrolases. *J. Am. Chem. Soc.* **129**, 9594–9595 (2007).

80. Thomas, G. et al. The serine hydrolase ABHD6 Is a critical regulator of the metabolic syndrome. *Cell Rep.* **5**, 508–520 (2013).
81. Christensen, R., Kristensen, P. K., Bartels, E. M., Bliddal, H. & Astrup, A. Efficacy and safety of the weight-loss drug rimonabant: a meta-analysis of randomised trials. *Lancet* **370**, 1706–1713 (2007).
82. Ohno-Shosaku, T. et al. Presynaptic cannabinoid sensitivity is a major determinant of depolarization-induced retrograde suppression at hippocampal synapses. *J. Neurosci.* **22**, 3864–3872 (2002).
83. Adermark, L., Talani, G. & Lovinger, D. M. Endocannabinoid-dependent plasticity at GABAergic and glutamatergic synapses in the striatum is regulated by synaptic activity. *Eur. J. Neurosci.* **29**, 32–41 (2009).
84. Singh, S. et al. ABHD6 selectively controls metabotropic-dependent increases in 2-AG production. *bioRxiv*, 2022.2005.2018.492553, https://doi.org/10.1101/2022.05.18.492553 (2022).
85. Busquets-Garcia, A., Bains, J. & Marsicano, G. CB1 receptor signaling in the brain: extracting specificity from ubiquity. *Neuropsychopharmacology* **43**, 4–20 (2018).
86. Schwenk, J. et al. High-resolution proteomics unravel architecture and molecular diversity of native AMPA receptor complexes. *Neuron* **74**, 621–633 (2012).
87. Wei, M. et al. α/β-Hydrolase domain-containing 6 (ABHD6) negatively regulates the surface delivery and synaptic function of AMPA receptors. *Proc. Natl Acad. Sci. USA* **113**, E2695–E2704 (2016).
88. Schwenk, J. et al. An ER assembly line of AMPA-receptors controls excitatory neurotransmission and its plasticity. *Neuron* **104**, 680–692.e689 (2019).
89. Sigel, E. et al. The major central endocannabinoid directly acts at GABA(A) receptors. *Proc. Natl Acad. Sci. USA* **108**, 18150–18155 (2011).
90. Naydenov, A. V. et al. ABHD6 blockade exerts antiepileptic activity in PTZ-induced seizures and in spontaneous seizures in R6/2 mice. *Neuron* **83**, 361–371 (2014).
91. Le Strat, Y. & Le Foll, B. Obesity and cannabis use: results from 2 representative national surveys. *Am. J. Epidemiol.* **174**, 929–933 (2011).
92. Thompson, C. A. & Hay, J. W. Estimating the association between metabolic risk factors and marijuana use in U.S. adults using data from the continuous National Health and Nutrition Examination Survey. *Ann. Epidemiol.* **25**, 486–491 (2015).
93. Penner, E. A., Buettner, H. & Mittleman, M. A. The impact of marijuana use on glucose, insulin, and insulin resistance among US adults. *Am. J. Med.* **126**, 583–589 (2013).
94. Smit, E. & Crespo, C. J. Dietary intake and nutritional status of US adult marijuana users: results from the Third National Health and Nutrition Examination Survey. *Public Health Nutr.* **4**, 781–786 (2001).
95. Rodondi, N., Pletcher, M. J., Liu, K., Hulley, S. B. & Sidney, S. Marijuana use, diet, body mass index, and cardiovascular risk factors (from the CARDIA Study). *Am. J. Cardiol.* **98**, 478–484 (2006).
96. Tripathi, B. R. et al. Decreased prevalence of diabetes in marijuana users: cross-sectional data from the National Health and Nutrition Examination Survey (NHANES) III. *BMJ Open* **2**, e000494 (2012).
97. Clark, T. M., Jones, J. M., Hall, A. G., Tabner, S. A. & Kmiec, R. L. Theoretical explanation for reduced body mass index and obesity rates in cannabis users. *Cannabis Cannabinoid Res.* **3**, 259–271 (2018).
98. Kirkham, T. C., Williams, C. M., Fezza, F. & Marzo, V. D. Endocannabinoid levels in rat limbic forebrain and hypothalamus in relation to fasting, feeding and satiation: stimulation of eating by 2-arachidonoyl glycerol. *Br. J. Pharmacol.* **136**, 550–557 (2002).
99. Soria-Gómez, E. et al. Pharmacological enhancement of the endocannabinoid system in the nucleus accumbens shell stimulates food intake and increases c-Fos expression in the hypothalamus. *Br. J. Pharm.* **151**, 1109–1116 (2007).
100. Bellocchio, L. et al. Bimodal control of stimulated food intake by the endocannabinoid system. *Nat. Neurosci.* **13**, 281–283 (2010).
101. Stratford, T. R. & Kelley, A. E. GABA in the nucleus accumbens shell participates in the central regulation of feeding behavior. *J. Neurosci.* **17**, 4434–4440 (1997).
102. Reynolds, S. M. & Berridge, K. C. Fear and feeding in the nucleus accumbens shell: rostrocaudal segregation of GABA-elicited defensive behavior versus eating behavior. *J. Neurosci.* **21**, 3261–3270 (2001).
103. Baldo, B. A., Alsene, K. M., Negron, A. & Kelley, A. E. Hyperphagia induced by GABAA receptor-mediated inhibition of the nucleus accumbens shell: dependence on intact neural output from the central amygdaloid region. *Behav. Neurosci.* **119**, 1195–1206 (2005).
104. Krause, M., German, P. W., Taha, S. A. & Fields, H. L. A pause in nucleus accumbens neuron firing is required to initiate and maintain feeding. *J. Neurosci.* **30**, 4746 (2010).
105. Reed, S. J. et al. Coordinated reductions in excitatory input to the nucleus accumbens underlie food consumption. *Neuron* **99**, 1260–1273.e1264 (2018).
106. Vachez, Y. M. et al. Ventral arkypallidal neurons inhibit accumbal firing to promote reward consumption. *Nat. Neurosci.* **24**, 379–390 (2021).
107. Richard, J. M. & Berridge, K. C. Nucleus accumbens dopamine/glutamate interaction switches modes to generate desire versus dread: D(1) alone for appetitive eating but D(1) and D(2) together for fear. *J. Neurosci.* **31**, 12866–12879 (2011).
108. O'Connor, E. C. et al. Accumbal D1R neurons projecting to lateral hypothalamus authorize feeding. *Neuron* **88**, 553–564 (2015).
109. Ledent, C. et al. Unresponsiveness to cannabinoids and reduced addictive effects of opiates in CB1 receptor knockout mice. *Science* **283**, 401–404 (1999).
110. Monory, K. et al. Genetic dissection of behavioural and autonomic effects of Δ9-Tetrahydrocannabinol in mice. *PLOS Biol.* **5**, e269 (2007).
111. Soria-Gomez, E. et al. Subcellular specificity of cannabinoid effects in striatonigral circuits. *Neuron* **109**, 1513–1526.e1511 (2021).
112. Onaivi, E. S., Chakrabarti, A., Gwebu, E. T. & Chaudhuri, G. Neurobehavioral effects of delta 9-THC and cannabinoid (CB1) receptor gene expression in mice. *Behav. Brain Res.* **72**, 115–125 (1995).
113. Long, J. Z. et al. Selective blockade of 2-arachidonoylglycerol hydrolysis produces cannabinoid behavioral effects. *Nat. Chem. Biol.* **5**, 37–44 (2009).
114. Shonesy, B. C. et al. CaMKII regulates diacylglycerol lipase-α and striatal endocannabinoid signaling. *Nat. Neurosci.* **16**, 456–463 (2013).
115. Alhouayek, M., Masquelier, J., Cani, P. D., Lambert, D. M. & Muccioli, G. G. Implication of the anti-inflammatory bioactive lipid prostaglandin D2-glycerol ester in the control of macrophage activation and inflammation by ABHD6. *Proc. Natl Acad. Sci. USA* **110**, 17558–17563 (2013).
116. Deng, L., Viray, K., Singh, S., Cravatt, B. & Stella, N. ABHD6 controls amphetamine-stimulated hyperlocomotion: involvement of CB(1) Receptors. *Cannabis Cannabinoid Res.* **7**, 188–198 (2022).
117. Mogenson, G. J., Jones, D. L. & Yim, C. Y. From motivation to action: functional interface between the limbic system and the motor system. *Prog. Neurobiol.* **14**, 69–97 (1980).
118. Yael, D., Tahary, O., Gurovich, B., Belelovsky, K. & Bar-Gad, I. Disinhibition of the nucleus accumbens leads to macro-scale

hyperactivity consisting of micro-scale behavioral segments encoded by striatal activity. *J. Neurosci.* **39**, 5897–5909 (2019).
119. Horne, E. A. et al. Downregulation of cannabinoid receptor 1 from neuropeptide Y interneurons in the basal ganglia of patients with Huntington's disease and mouse models. *Eur. J. Neurosci.* **37**, 429–440 (2013).
120. Bonm, A. V. et al. Control of exploration, motor coordination and amphetamine sensitization by cannabinoid CB(1) receptors expressed in medium spiny neurons. *Eur. J. Neurosci.* **54**, 4934–4952 (2021).
121. Mariani, Y. et al. Striatopallidal cannabinoid type-1 receptors mediate amphetamine-induced sensitization. *Curr. Biol.*, https://doi.org/10.1016/j.cub.2023.09.075 (2023).
122. Schall, T. A., Wright, W. J. & Dong, Y. Nucleus accumbens fast-spiking interneurons in motivational and addictive behaviors. *Mol. Psychiatry* **26**, 234–246 (2021).
123. Manz, K. M. et al. Calcium-permeable AMPA receptors promote endocannabinoid signaling at Parvalbumin Interneuron synapses in the nucleus accumbens core. *Cell Rep.* **32**, 107971 (2020).
124. Manz, K. M. et al. Cocaine restricts nucleus accumbens feedforward drive through a monoamine-independent mechanism. *Neuropsychopharmacology* **47**, 652–663 (2022).
125. Owen, S. F., Berke, J. D. & Kreitzer, A. C. Fast-spiking interneurons supply feedforward control of bursting, calcium, and plasticity for efficient learning. *Cell* **172**, 683–695.e615 (2018).
126. Wiltschko, A. B., Pettibone, J. R. & Berke, J. D. Opposite effects of stimulant and antipsychotic drugs on striatal fast-spiking interneurons. *Neuropsychopharmacology* **35**, 1261–1270 (2010).
127. Morra, J. T., Glick, S. D. & Cheer, J. F. Neural encoding of psychomotor activation in the nucleus accumbens core, but not the shell, requires cannabinoid receptor signaling. *J. Neurosci.* **30**, 5102–5107 (2010).
128. Roberts, B. M., White, M. G., Patton, M. H., Chen, R. & Mathur, B. N. Ensemble encoding of action speed by striatal fast-spiking interneurons. *Brain Struct. Funct.* **224**, 2567–2576 (2019).
129. Gritton, H. J. et al. Unique contributions of parvalbumin and cholinergic interneurons in organizing striatal networks during movement. *Nat. Neurosci.* **22**, 586–597 (2019).
130. Pennartz, C. M., Groenewegen, H. J. & Lopes da Silva, F. H. The nucleus accumbens as a complex of functionally distinct neuronal ensembles: an integration of behavioural, electrophysiological and anatomical data. *Prog. Neurobiol.* **42**, 719–761 (1994).
131. Roseberry, T. K. et al. Cell-type-specific control of brainstem locomotor circuits by basal Ganglia. *Cell* **164**, 526–537 (2016).
132. Leiras, R., Cregg, J. M. & Kiehn, O. Brainstem circuits for locomotion. *Annu Rev. Neurosci.* **45**, 63–85 (2022).
133. Salamone, J. D. & Correa, M. The mysterious motivational functions of mesolimbic dopamine. *Neuron* **76**, 470–485 (2012).
134. Beeler, J. A., Frazier, C. R. & Zhuang, X. Putting desire on a budget: dopamine and energy expenditure, reconciling reward and resources. *Front Integr. Neurosci.* **6**, 49 (2012).
135. Salamone, J. D. et al. Haloperidol and nucleus accumbens dopamine depletion suppress lever pressing for food but increase free food consumption in a novel food choice procedure. *Psychopharmacology* **104**, 515–521 (1991).
136. Salamone, J. D., Cousins, M. S. & Bucher, S. Anhedonia or anergia? Effects of haloperidol and nucleus accumbens dopamine depletion on instrumental response selection in a T-maze cost/benefit procedure. *Behav. Brain Res.* **65**, 221–229 (1994).
137. Schelp, S. A. et al. A transient dopamine signal encodes subjective value and causally influences demand in an economic context. *Proc. Natl Acad. Sci. USA* **114**, E11303–e11312 (2017).
138. Koob, G. F., Riley, S. J., Smith, S. C. & Robbins, T. W. Effects of 6-hydroxydopamine lesions of the nucleus accumbens septi and olfactory tubercle on feeding, locomotor activity, and amphetamine anorexia in the rat. *J. Comp. Physiol. Psychol.* **92**, 917–927 (1978).
139. Salamone, J. D., Kurth, P. A., McCullough, L. D., Sokolowski, J. D. & Cousins, M. S. The role of brain dopamine in response initiation: effects of haloperidol and regionally specific dopamine depletions on the local rate of instrumental responding. *Brain Res.* **628**, 218–226 (1993).
140. Baldo, B. A., Sadeghian, K., Basso, A. M. & Kelley, A. E. Effects of selective dopamine D1 or D2 receptor blockade within nucleus accumbens subregions on ingestive behavior and associated motor activity. *Behav. Brain Res.* **137**, 165–177 (2002).
141. Haney, M. et al. Signaling-specific inhibition of the CB1 receptor for cannabis use disorder: phase 1 and phase 2a randomized trials. *Nat. Med.* **29**, 1487–1499 (2023).
142. Higgs, S., Barber, D. J., Cooper, A. J. & Terry, P. Differential effects of two cannabinoid receptor agonists on progressive ratio responding for food and free-feeding in rats. *Behav. Pharm.* **16**, 389–393 (2005).
143. Solinas, M. & Goldberg, S. R. Motivational effects of cannabinoids and opioids on food reinforcement depend on simultaneous activation of cannabinoid and opioid systems. *Neuropsychopharmacology* **30**, 2035–2045 (2005).
144. Ward, S. J. & Dykstra, L. A. The role of CB1 receptors in sweet versus fat reinforcement: effect of CB1 receptor deletion, CB1 receptor antagonism (SR141716A) and CB1 receptor agonism (CP-55940). *Behav. Pharm.* **16**, 381–388 (2005).
145. Randall, P. A. et al. Dopaminergic modulation of effort-related choice behavior as assessed by a progressive ratio chow feeding choice task: pharmacological studies and the role of individual differences. *PLoS One* **7**, e47934 (2012).
146. Randall, P. A. et al. The VMAT-2 inhibitor tetrabenazine affects effort-related decision making in a progressive ratio/chow feeding choice task: reversal with antidepressant drugs. *PLoS One* **9**, e99320 (2014).
147. Thornton-Jones, Z. D., Vickers, S. P. & Clifton, P. G. The cannabinoid CB1 receptor antagonist SR141716A reduces appetitive and consummatory responses for food. *Psychopharmacology* **179**, 452–460 (2005).
148. Rasmussen, E. B. & Huskinson, S. L. Effects of rimonabant on behavior maintained by progressive ratio schedules of sucrose reinforcement in obese Zucker (fa/fa) rats. *Behav. Pharm.* **19**, 735–742 (2008).
149. Maccioni, P., Pes, D., Carai, M. A., Gessa, G. L. & Colombo, G. Suppression by the cannabinoid CB1 receptor antagonist, rimonabant, of the reinforcing and motivational properties of a chocolate-flavoured beverage in rats. *Behav. Pharm.* **19**, 197–209 (2008).
150. Mateo, Y. et al. Endocannabinoid actions on cortical terminals orchestrate local modulation of dopamine release in the nucleus accumbens. *Neuron* **96**, 1112–1126.e1115 (2017).
151. Ramiro-Fuentes, S., Ortiz, O., Moratalla, R. & Fernandez-Espejo, E. Intra-accumbens rimonabant is rewarding but induces aversion to cocaine in cocaine-treated rats, as does in vivo accumbal cannabinoid CB1 receptor silencing: critical role for glutamate receptors. *Neuroscience* **167**, 205–215 (2010).
152. Norris, C., Szkudlarek, H. J., Pereira, B., Rushlow, W. & Laviolette, S. R. The bivalent rewarding and aversive properties of δ(9)-tetrahydrocannabinol are mediated through dissociable opioid receptor substrates and neuronal modulation mechanisms in distinct striatal sub-regions. *Sci. Rep.* **9**, 9760 (2019).
153. Voorn, P., Vanderschuren, L. J., Groenewegen, H. J., Robbins, T. W. & Pennartz, C. M. Putting a spin on the dorsal-ventral divide of the striatum. *Trends Neurosci.* **27**, 468–474 (2004).
154. Grueter, B. A., Brasnjo, G. & Malenka, R. C. Postsynaptic TRPV1 triggers cell type-specific long-term depression in the nucleus accumbens. *Nat. Neurosci.* **13**, 1519–1525 (2010).

155. Bilbao, A. et al. Endocannabinoid LTD in accumbal D1 neurons mediates reward-seeking behavior. *iScience* **23**, 100951 (2020).
156. Augustin, S. M., Gracias, A. L., Luo, G., Anumola, R. C. & Lovinger, D. M. Striatonigral direct pathway 2-arachidonoylglycerol contributes to ethanol effects on synaptic transmission and behavior. *Neuropsychopharmacology*, https://doi.org/10.1038/s41386-023-01671-8 (2023).
157. Zhang, H. Y. et al. Cannabinoid CB2 receptors modulate midbrain dopamine neuronal activity and dopamine-related behavior in mice. *Proc. Natl Acad. Sci. USA* **111**, E5007–E5015 (2014).
158. Foster, D. J. et al. Antipsychotic-like effects of M4 positive allosteric modulators are mediated by CB2 receptor-dependent inhibition of dopamine release. *Neuron* **91**, 1244–1252 (2016).
159. Gantz, S. C. & Bean, B. P. Cell-autonomous excitation of midbrain dopamine neurons by Endocannabinoid-dependent lipid signaling. *Neuron* **93**, 1375–1387.e1372 (2017).
160. Pribasnig, M. A. et al. α/β hydrolase domain-containing 6 (ABHD6) Degrades the Late Endosomal/Lysosomal Lipid Bis(monoacylglycero)phosphate. *J. Biol. Chem.* **290**, 29869–29881 (2015).
161. Ogasawara, D. et al. Rapid and profound rewiring of brain lipid signaling networks by acute diacylglycerol lipase inhibition. *Proc. Natl Acad. Sci.* **113**, 26–33 (2016).
162. Cristino, L., Bisogno, T. & Di Marzo, V. Cannabinoids and the expanded endocannabinoid system in neurological disorders. *Nat. Rev. Neurol.* **16**, 9–29 (2020).
163. Singh, S. et al. Pharmacological Characterization of the Endocannabinoid Sensor GRAB(eCB2.0). *Cannabis Cannabinoid Res*, https://doi.org/10.1089/can.2023.0036 (2023).
164. Ortega-Gutiérrez, S., Hawkins, E. G., Viso, A., López-Rodríguez, M. L. & Cravatt, B. F. Comparison of anandamide transport in FAAH wild-type and knockout neurons: evidence for contributions by both FAAH and the CB1 receptor to anandamide uptake. *Biochemistry* **43**, 8184–8190 (2004).
165. Robbe, D., Alonso, G., Duchamp, F., Bockaert, J. & Manzoni, O. J. Localization and mechanisms of action of cannabinoid receptors at the glutamatergic synapses of the mouse nucleus accumbens. *J. Neurosci.* **21**, 109–116 (2001).
166. Hoffman, A. F. & Lupica, C. R. Direct actions of cannabinoids on synaptic transmission in the nucleus accumbens: a comparison with opioids. *J. Neurophysiol.* **85**, 72–83 (2001).
167. Walter, L., Dinh, T. & Stella, N. ATP induces a rapid and pronounced increase in 2-arachidonoylglycerol production by astrocytes, a response limited by monoacylglycerol lipase. *J. Neurosci.* **24**, 8068–8074 (2004).
168. Viader, A. et al. Metabolic interplay between astrocytes and neurons regulates Endocannabinoid action. *Cell Rep.* **12**, 798–808 (2015).
169. Martín, R., Bajo-Grañeras, R., Moratalla, R., Perea, G. & Araque, A. Circuit-specific signaling in astrocyte-neuron networks in basal ganglia pathways. *Science* **349**, 730–734 (2015).
170. Requie, L. M. et al. Astrocytes mediate long-lasting synaptic regulation of ventral tegmental area dopamine neurons. *Nat. Neurosci.* **25**, 1639–1650 (2022).
171. Zhao, S. et al. α/β-Hydrolase domain-6 and saturated long chain monoacylglycerol regulate insulin secretion promoted by both fuel and non-fuel stimuli. *Mol. Metab.* **4**, 940–950 (2015).
172. Sharma, S., Hryhorczuk, C. & Fulton, S. Progressive-ratio responding for palatable high-fat and high-sugar food in mice. *J. Vis. Exp.*, e3754, https://doi.org/10.3791/3754 (2012).
173. Stauffer, W. R. et al. Dopamine neuron-specific optogenetic stimulation in Rhesus Macaques. *Cell* **166**, 1564–1571.e1566 (2016).
174. Hryhorczuk, C. et al. Dampened mesolimbic dopamine function and signaling by saturated but not monounsaturated dietary lipids. *Neuropsychopharmacology* **41**, 811–821 (2016).
175. Décarie-Spain, L. et al. Nucleus accumbens inflammation mediates anxiodepressive behavior and compulsive sucrose seeking elicited by saturated dietary fat. *Mol. Metab.* **10**, 1–13 (2018).
176. Sharma, S. & Fulton, S. Diet-induced obesity promotes depressive-like behaviour that is associated with neural adaptations in brain reward circuitry. *Int J. Obes.* **37**, 382–389 (2013).
177. Andersen, C. L., Jensen, J. L. & Ørntoft, T. F. Normalization of real-time quantitative reverse transcription-PCR data: a model-based variance estimation approach to identify genes suited for normalization, applied to bladder and colon cancer data sets. *Cancer Res* **64**, 5245–5250 (2004).
178. Zoerner, A. A. et al. Simultaneous UPLC-MS/MS quantification of the endocannabinoids 2-arachidonoyl glycerol (2AG), 1-arachidonoyl glycerol (1AG), and anandamide in human plasma: minimization of matrix-effects, 2AG/1AG isomerization and degradation by toluene solvent extraction. *J. Chromatogr. B Anal. Technol. Biomed. Life Sci.* **883-884**, 161–171 (2012).

Acknowledgements

This work was supported by a pilot grant from Montreal Diabetes Research Centre-Diabète Québec and project grant from the Canadian Institutes of Health Research (CIHR, MOP123280) to S.F., T.A. and D.S. D.L. was supported by MSc and PhD scholarships from the Fonds de Recherche Québec Santé (FRQS). S.T. was supported by postdoctoral fellowships from Diabète Québec and the CRCHUM. AF held a Canadian Diabetes Association postdoctoral fellowship. S.F. and T.A. were supported by salary awards from FRQS. We thank the Metabolic Phenotyping Core of CRCHUM for permission to use ECHO MRI and CLAMS apparatus and Demetra Rodaros, Victor Ernesto Issa Garcia (Mitacs Globalink Internship) and José Iglesias for their technical assistance.

Author contributions

D.L., S.T. and S.F. designed studies. S.T., D.L., S.N., A.F., D.M., and A.K.F.F. performed in vivo and biochemical experiments. H.P. and D.S. provided electrophysiological expertise and H.P. performed experiments. M.-L.P. performed HPLC tandem MS/MS experiments. S.T., D.L., H.P., D.M., A.K.F.F., M.-L.P., and S.F. analyzed data. M.P. and S.R.M.M. initiated discussions of studying brain ABHD6 and provided initial *Abhd6*$^{lox/lox}$ mice. T.A. provided guidance in experimental design and interpretation. D.L., S.T., and S.F. wrote the manuscript. All authors critically reviewed the manuscript.

Competing interests

The authors declare no competing interests.

Additional information

Supplementary information The online version contains supplementary material available at https://doi.org/10.1038/s41467-024-54819-5.

Correspondence and requests for materials should be addressed to Stephanie Fulton.

Peer review information *Nature Communications* thanks John Salamone and the other, anonymous, reviewers for their contribution to the peer review of this work. A peer review file is available.

Reprints and permissions information is available at http://www.nature.com/reprints

Publisher's note Springer Nature remains neutral with regard to jurisdictional claims in published maps and institutional affiliations.

Open Access This article is licensed under a Creative Commons Attribution-NonCommercial-NoDerivatives 4.0 International License, which permits any non-commercial use, sharing, distribution and reproduction in any medium or format, as long as you give appropriate credit to the original author(s) and the source, provide a link to the Creative Commons licence, and indicate if you modified the licensed material. You do not have permission under this licence to share adapted material derived from this article or parts of it. The images or other third party material in this article are included in the article's Creative Commons licence, unless indicated otherwise in a credit line to the material. If material is not included in the article's Creative Commons licence and your intended use is not permitted by statutory regulation or exceeds the permitted use, you will need to obtain permission directly from the copyright holder. To view a copy of this licence, visit http://creativecommons.org/licenses/by-nc-nd/4.0/.

© The Author(s) 2024